PUBLICATIONS OF THE ASTRONOMICAL SOCIETY OF THE PACIFIC, **115**:763–795, 2003 July

Invited Review

Galactic Stellar and Substellar Initial Mass Function[1]

GILLES CHABRIER

Ecole Normale Supérieure de Lyon, Centre de Recherche Astrophysique de Lyon, UMR CNRS 5574, 69364 Lyon Cedex 07, France; chabrier@ens-lyon.fr

Received 2003 March 31; accepted 2003 March 31

ABSTRACT. We review recent determinations of the present-day mass function (PDMF) and initial mass function (IMF) in various components of the Galaxy—disk, spheroid, young, and globular clusters—and in conditions characteristic of early star formation. As a general feature, the IMF is found to depend weakly on the environment and to be well described by a power-law form for $m \gtrsim 1\ M_\odot$ and a lognormal form below, except possibly for early star formation conditions. The disk IMF for single objects has a characteristic mass around $m_c \sim 0.08\ M_\odot$ and a variance in logarithmic mass $\sigma \sim 0.7$, whereas the IMF for multiple systems has $m_c \sim 0.2\ M_\odot$ and $\sigma \sim 0.6$. The extension of the single MF into the brown dwarf regime is in good agreement with present estimates of L- and T-dwarf densities and yields a disk brown dwarf number density comparable to the stellar one, $n_{\rm BD} \sim n_* \sim 0.1\ {\rm pc}^{-3}$. The IMF of young clusters is found to be consistent with the disk field IMF, providing the same correction for unresolved binaries, confirming the fact that young star clusters and disk field stars represent the same stellar population. Dynamical effects, yielding depletion of the lowest mass objects, are found to become consequential for ages $\gtrsim$130 Myr. The spheroid IMF relies on much less robust grounds. The large metallicity spread in the local subdwarf photometric sample, in particular, remains puzzling. Recent observations suggest that there is a continuous kinematic shear between the thick-disk population, present in local samples, and the genuine spheroid one. This enables us to derive only an upper limit for the spheroid mass density and IMF. Within all the uncertainties, the latter is found to be similar to the one derived for globular clusters and is well represented also by a lognormal form with a characteristic mass slightly larger than for the disk, $m_c \sim 0.2$–$0.3\ M_\odot$, excluding a significant population of brown dwarfs in globular clusters and in the spheroid. The IMF characteristic of early star formation at large redshift remains undetermined, but different observational constraints suggest that it does not extend below $\sim 1\ M_\odot$. These results suggest a characteristic mass for star formation that decreases with time, from conditions prevailing at large redshift to conditions characteristic of the spheroid (or thick disk) to present-day conditions. These conclusions, however, remain speculative, given the large uncertainties in the spheroid and early star IMF determinations.

These IMFs allow a reasonably robust determination of the Galactic present-day and initial stellar and brown dwarf contents. They also have important galactic implications beyond the Milky Way in yielding more accurate mass-to-light ratio determinations. The mass-to-light ratios obtained with the disk and the spheroid IMF yield values 1.8–1.4 times smaller than for a Salpeter IMF, respectively, in agreement with various recent dynamical determinations. This general IMF determination is examined in the context of star formation theory. None of the theories based on a Jeans-type mechanism, where fragmentation is due only to gravity, can fulfill all the observational constraints on star formation and predict a large number of substellar objects. On the other hand, recent numerical simulations of compressible turbulence, in particular in super-Alfvénic conditions, seem to reproduce both qualitatively and quantitatively the stellar and substellar IMF and thus provide an appealing theoretical foundation. In this picture, star formation is induced by the dissipation of large-scale turbulence to smaller scales through radiative MHD shocks, producing filamentary structures. These shocks produce local nonequilibrium structures with large density contrasts, which collapse eventually in gravitationally bound objects under the combined influence of turbulence and gravity. The concept of a single Jeans mass is replaced by a distribution of local Jeans masses, representative of the lognormal probability density function of the turbulent gas. Objects below the mean thermal Jeans mass still have a possibility to collapse, although with a decreasing probability.

[1] The page charges for this Review were partially covered by a generous gift from a *PASP* supporter.

1. INTRODUCTION

1.1. Historical Perspective

Since the pioneering paper of Salpeter (1955), several fundamental reviews on the Galactic stellar mass function (MF) have been written by, in particular, Schmidt (1959), Miller & Scalo (1979, hereafter MS79), and Scalo (1986). A shorter, more recent discussion is given by Kroupa (2002). The determination of the stellar MF is a cornerstone in astrophysics, for the stellar mass distribution determines the evolution, surface brightness, chemical enrichment, and baryonic content of galaxies. Determining whether this MF has been constant along the evolution of the universe or varies with redshift bears crucial consequences on the so-called cosmic star formation, i.e., on the universe's light and matter evolution. Furthermore, the knowledge of the MF in our Galaxy yields the complete census of its stellar and substellar population and provides an essential diagnostic to understand the formation of starlike objects. As emphasized by Scalo (1986), the stellar and substellar mass distribution is the link between stellar and galactic evolution.

As is too rarely stressed, there is no direct observational determination of the MF. What is observed is the individual or integrated light of objects, i.e., the luminosity function (LF) or the surface brightness. Transformation of this observable quantity into the MF thus relies on theories of stellar evolution, and more precisely, on the relationship between mass, age, and light, i.e., mass-age-luminosity relations.

Until recently, only the LFs of giants and Sun-like stars, i.e., objects with mass $m \gtrsim 1\ M_{\odot}$, were observed with enough precision to derive stellar MFs. The latter were presented as power-law approximations, $dN/dm \propto m^{-\alpha}$, as initially suggested by Salpeter (1955), with an exponent close to the Salpeter value $\alpha = 2.35$. A departure from this monotonic behavior, with a flattening of the MF below $\sim 1\ M_{\odot}$, was first proposed by MS79, who suggested a lognormal form. The tremendous progress realized within the past few years from the observational side, from both ground-based and space-based surveys, now probes the M-dwarf stellar distribution down to the bottom of the main sequence (MS). Moreover, over 100 brown dwarfs have now been discovered, both in the Galactic field and in young clusters, down to a few Jupiter masses, providing important constraints on the census of substellar objects in the Galaxy, not to mention the ongoing detection of planets orbiting stars outside our solar system. All these recent discoveries show unambiguously that the stellar MF extends well below the hydrogen- and probably the deuterium-burning limit and urge a revised determination of the stellar and substellar census in the Galaxy and thus of its MF. In the meantime, the general theory of low-mass star and brown dwarf evolution has now reached a mature state, allowing a reasonably robust description of the mechanical and thermal properties of these complex objects and of their observational signatures.

It is the purpose of this review to summarize these recent discoveries, to examine which lessons from the Milky Way can be applied to a more general galactic and cosmological context, and to determine our present knowledge of the Galactic MF and our present understanding of star formation. Detailed discussions on the MF of massive stars ($m \gtrsim 1\ M_{\odot}$) have been developed in the remarkable reviews of MS79 and Scalo (1986), and we orient the reader to these papers for these objects. The present review will focus on the low-mass part of the MF in various regions of the Galaxy and its extension into the substellar regime. Low-mass stars (hereafter stars with mass $m < 1\ M_{\odot}$) have effective temperatures $T_{\rm eff} \lesssim 6000$ K, which implies eventually formation of molecules in their atmosphere. Below $T_{\rm eff} \sim 4000$ K, their spectral energy distribution strongly departs from a blackbody distribution and peaks generally in the visible or near-infrared, with yellow to red colors (see Chabrier & Baraffe 2000 for a recent review). These objects live for a Hubble time or longer and provide the overwhelming majority of the Galactic stellar contents.

The organization of the paper is as follows: in § 1, we summarize the various definitions used in the present review and briefly summarize our present knowledge, and the remaining uncertainties, of the mass-magnitude relationship. Sections 2–5 are devoted, respectively, to the determination of the MFs for the Galactic field and young clusters, Galactic spheroids, globular clusters, and dark halo and early stars. The stellar and substellar Galactic mass budget and the cosmological implications are presented in § 6. Examination of our present understanding of star formation is discussed in § 7, while § 8 is devoted to the conclusions.

1.2. Definitions

1.2.1. Mass Function

The MF was originally defined by Salpeter (1955) as the number of stars N in a volume of space V observed at a time t per logarithmic mass interval $d \log m$:

$$\xi(\log m) = \frac{d(N/V)}{d \log m} = \frac{dn}{d \log m}, \qquad (1)$$

where $n = N/V$ is the stellar number density, which is in pc^{-3} in the following.

This definition was used also by MS79[2] and Scalo (1986). Since the formation of starlike objects is now observed to take place over 5 orders of magnitude in mass, from about 100 to $10^{-3}\ M_{\odot}$, such a logarithmic definition of the MF seems to be the most satisfactory representation of the mass distribution in

[2] Note that Miller & Scalo use the stellar *surface* density, in pc^{-2}, in their definition of the MF, to be divided by the respective Galactic scale heights of the various stellar populations to get the volume density in the solar neighborhood.

the Galaxy. Conversely, Scalo (1986) defines the *mass spectrum* as the number density distribution per mass interval dn/dm with the obvious relation

$$\xi(m) = \frac{dn}{dm} = \frac{1}{m(\ln 10)}\,\xi(\log m). \tag{2}$$

With these definitions, if the MF is approximated as a power law, the exponents are usually denoted, respectively, x and α, with $\xi(\log m) \propto m^{-x}$ and $\xi(m) \propto m^{-\alpha}$, $x = \alpha - 1$. The original Salpeter value is $x = 1.35$, $\alpha = 2.35$.

Stars eventually evolve off the MS after a certain age, so the present-day MF (PDMF) of MS stars, which can be determined from the observed present-day LF, differs from the so-called *initial* mass function (IMF), i.e., the number of stars that were originally created per mass interval in the Galaxy. Indeed, stars with masses above the minimum so-called turnoff mass will have evolved as red giants and white dwarfs or neutron stars or black holes as the end product of Type II supernovae explosions, depending on the initial MS mass. Here the minimum turnoff mass is defined as the mass for which the age at which the star starts evolving off the MS on the giant branch equals the age of the Galaxy (or the age of a given cluster). For an age $\tau_D \approx 10$ Gyr, about the age of the Galactic disk, this corresponds to a mass $m_{\rm TO} \approx 0.9\ M_\odot$ for solar metallicity. The determination of the PDMF thus involves the star formation rate (SFR) $b(t)$, i.e., the number of stars (more generically starlike objects) formed per time interval along galactic evolution. For this reason, the quantity to be considered to link the PDMF and IMF is the so-called stellar creation function, as introduced by MS79.

1.2.2. Creation Function

The creation function $C(\log m,\ t)$ is defined as the number of stars per unit volume formed in the mass range ($\log m$, $\log m + d\log m$) during the time interval (t, $t + dt$). Given this definition, the total number of starlike objects per unit volume *ever formed* in the Galaxy reads

$$n_{\rm tot} = \int_{\log(m_{\rm inf})}^{\log(m_{\rm sup})} \int_0^{\tau_{\rm G}} C(\log m,\ t)\, d\log m\, dt, \tag{3}$$

where $m_{\rm inf}$ and $m_{\rm sup}$ denote, respectively, the minimum and maximum mass for the formation of starlike objects, and $\tau_{\rm G}$ denotes the age of the Galaxy.[3]

The creation function is related to the total birthrate $B(t)$, i.e., the total number density of starlike objects ever formed per *unit time*, as

$$B(t) = \int_{\log(m_{\rm inf})}^{\log(m_{\rm sup})} C(\log m,\ t)\, d\log m. \tag{4}$$

Following MS79, we refer to the SFR as the ratio of the absolute birthrate at time t over the average birthrate:

$$b(t) = \frac{B(t)}{(1/\tau_{\rm G})\int_0^{\tau_{\rm G}} B(t)\, dt}, \tag{5}$$

so $\int_0^{\tau_{\rm G}} b(t)\, dt = \tau_{\rm G}$.

It is generally admitted that the creation function can be separated into the product of a function of mass—the mass function—and a function of time—the formation rate. The underlying physical hypothesis is that the MF, the issue of the physical process that drives star formation per mass interval, does not depend on time. In fact, as will be illustrated later on, time may play a role in this mechanism in determining some characteristic mass, but without affecting the generic form of $\xi(m)$. Under such a condition of separability of mass and time, the creation function $C(m,\ t)$ can be rewritten

$$C(\log m,\ t) = \xi(\log m)\,\frac{B(t)}{\int_0^{\tau_{\rm G}} B(t)\, dt} = \xi(\log m)\,\frac{b(t)}{\tau_{\rm G}}. \tag{6}$$

The IMF, i.e., the total number density of starlike objects *ever formed* per unit log mass, thus reads

$$\xi(\log m) = \int_0^{\tau_{\rm G}} C(\log m,\ t)\, dt. \tag{7}$$

From equations (3) and (5), the IMF and the SFR are related to the total number density of starlike objects ever formed in the Galaxy by

$$\begin{aligned} n_{\rm tot}(t = \tau_{\rm G}) &= \frac{1}{\tau_{\rm G}} \int_0^{\tau_{\rm G}} b(t)\, dt \int_{\log(m_{\rm inf})}^{\log(m_{\rm sup})} \xi(\log m)\, d\log m \\ &= \int_{\log(m_{\rm inf})}^{\log(m_{\rm sup})} \xi(\log m)\, d\log m. \end{aligned} \tag{8}$$

As noted by MS79, all stars with MS lifetimes greater than the age of the Galaxy are still on the MS. In that case, the PDMF and the IMF are equivalent. This holds for brown dwarfs (BDs) too. Brown dwarfs have unlimited lifetimes, so all BDs ever formed in the Galaxy still exist today, regardless of when they were formed, and the BD PDMF is the BD IMF. For stars with MS lifetimes $\tau_{\rm MS}$ less than the age of the Galaxy, only those within the last $\tau_{\rm MS}$ are observed today as MS stars. In that case, the PDMF $\phi_{\rm MS}(\log m)$ and the IMF $\xi(\log m)$ are different and—using the separability condition for the creation

[3] Or the age of a given cluster if one wants to determine a cluster stellar content.

function—obey the condition (MS79)

$$\phi_{\rm MS}(\log m) = \frac{\xi(\log m)}{\tau_{\rm G}} \int_{\tau_{\rm G}-\tau_{\rm MS}}^{\tau_{\rm G}} b(t)\, dt,\ \tau_{\rm MS} < \tau_{\rm G}. \quad (9)$$

1.2.3. Functional Forms

The most widely used functional form for the MF is the power law, as suggested originally by Salpeter (1955):

$$\xi(\log m) = Am^{-x}. \quad (10)$$

This form is believed to adequately describe the IMF of massive stars in our Galaxy, $m \gtrsim 1\ M_\odot$, with an exponent $x \simeq 1.7$ (Scalo 1986, Table VII), for a standard fraction of observationally unresolved binaries (Kroupa 2001). Uncertainties remain, however, in the exact value of the exponent, and a Salpeter exponent $x = 1.3$ seems to be more consistent with the measured light from high-z galaxies. This issue will be discussed in § 6. The PDMF of massive stars has been calculated by Scalo (1986, Table IV), and the corresponding volume-density distribution is adequately fitted by the following three-segment power law:

$$\begin{aligned} x &= 4.37,\ 0 \le \log m \le 0.54, \\ x &= 3.53,\ 0.54 \le \log m \le 1.26, \\ x &= 2.11,\ 1.26 \le \log m \le 1.80, \end{aligned} \quad (11)$$

with the respective normalization constants $A = 0.044$, 0.015, and $2.5 \times 10^{-4}\ (\log M_\odot)^{-1}\ {\rm pc}^{-3}$. Note that this MF denotes the *volume* density of objects $\rm pc^{-3}$ per interval of log m, where the surface density has been transformed in volume density using the Scalo (1986) mass-dependent scale heights. The distinctive property of a power-law MF is that it has no preferred mass scale, as will be discussed in § 7.

The second widely used form is the normal, or Gaussian, distribution, as suggested by MS79:

$$\xi(\log m) = \frac{A}{\sqrt{2\pi}\sigma} \exp\left[-\frac{(\log m - \log m_c)^2}{2\sigma^2}\right], \quad (12)$$

where $\log m_c$ and $\sigma^2 = \langle(\log m - \langle\log m\rangle)^2\rangle$ denote, respectively, the mean mass and the variance in log m.

A third, more general form, is the so-called generalized Rosin-Rammler function:

$$\xi(\log m) = Am^{-x} \exp\left[-\left(\frac{B}{m}\right)^\beta\right], \quad \beta > 0. \quad (13)$$

This form recovers asymptotically a power law at large m, $\xi(\log m)_{m\to\infty} \to m^{-x}$, and resembles a lognormal form in the other limit, with a peak value at $m_p = B(\beta/x)^{1/\beta}$. The case $\beta = 0$ corresponds to the power law.

In terms of statistical physics, the MF can be interpreted as a probability density function $p(m) = \xi(m)/n_{\rm tot}$ and thus a probability density

$$\int_{m_{\rm inf}}^{m_{\rm sup}} p(m)\, dm = 1, \quad (14)$$

with the probability for a star to have a mass $\in (m_{\rm inf}, m)$:

$$P(m) = \int_{m_{\rm inf}}^{m} p(x)\, dx = \frac{1}{n_{\rm tot}} \int_{m_{\rm inf}}^{m} \xi(x)\, dx. \quad (15)$$

1.3. Mass-Magnitude Relationships

The only possible direct determination of a stellar mass is by use of Kepler's third law in a binary system, providing a long enough time basis to get the appropriate dynamical information. As shown below, the statistics of such a sample is largely insufficient to allow a reasonable estimate of the MF, but it certainly provides stringent constraints for the models. Therefore, as mentioned earlier, the only possible way to determine a PDMF is by transformation of an observed LF $\Phi = dN/dM$, i.e., the number of stars N per absolute magnitude interval dM, into an MF. This involves the derivative of a mass-luminosity relationship for a given age τ, or preferentially of a mass-magnitude relationship (MMR), which applies directly in the observed magnitude and avoids the use of often ill-determined bolometric corrections:

$$\frac{dn}{dm}(m)_\tau = \left[\frac{dn}{dM_\lambda(m)}\right]\left[\frac{dm}{dM_\lambda(m)}\right]_\tau^{-1}, \quad (16)$$

where M_λ denotes the absolute magnitude in a given bandpass. Another way to proceed is to attribute a mass to each star of the sample, which avoids involving explicitly the derivative of the MMR. In practice, both methods should yield similar results.

A first compilation of mass-luminosity data in the M-dwarf domain was published by Popper (1980) and was subsequently extended by Henry & McCarthy (1993), who used speckle interferometry to obtain MMRs in the V, J, H, and K bands. The determination of the V magnitude was improved subsequently with the *Hubble Space Telescope* (*HST*; Henry et al. 1999), reducing appreciably the uncertainty in the m-M_V relation. This sample has been improved significantly recently by Delfosse et al. (2000) and Ségransan et al. (2003b). Combining adaptive-optics images and accurate radial velocities, these authors determined the MMRs of about 20 objects between ~0.6 and ~0.09 $M_\odot$ in the aforementioned bands with mass accuracies of 0.2%–5%.

The MMRs derived from the Baraffe et al. (1998, hereafter

BCAH98) models reproduce the Delfosse et al. (2000) and Ségransan et al. (2003b) data over the entire aforementioned mass range in the J, H, and K bands within less than 1 σ (see Fig. 3 of Delfosse et al. 2000). The agreement is not as good in the V band, with a systematic offset of a few tenths of a magnitude between theory and observation below $\sim$0.3 $M_\odot$, $M_V \gtrsim 12$. In terms of mass determination for a given M_V, however, the effect remains modest, with a maximum 15% error on the mass determined with the theoretical MMR around magnitude $M_V \sim 12$–13 (Chabrier 2001, Figs. 1 and 2). Using the Very Large Telescope Interferometer (VLTI), Ségransan et al. (2003a) obtained accurate radius measurements for some of the aforementioned very low mass objects. The theoretical calculations (BACH98) agree within 1% or less for $m \leq 0.5\ M_\odot$. No BD eclipsing binary has been detected yet, so theoretical masses cannot be compared directly with observation for BDs (assuming that the age of the system is well determined, a mandatory condition for BDs). However, the observation of multiple systems believed to be coeval, with dynamically determined total mass and with components extending well into the BD domain, provides stringent constraints on the theory (White et al. 1999). The recent observations of different color-magnitude diagrams of young clusters that extend down to Jupiter-like objects (Zapatero Osorio et al. 2000; Béjar et al. 2001; Lucas et al. 2001; Martín et al. 2001) provide another precious constraint. The BCAH98 models successfully reproduce all these observations along one isochrone (see references above). One must remain cautious, however, about the exact accuracy of the models in the substellar domain, given the lack of precise constraints. A recent analysis by Dobbie et al. (2002c) seems to suggest an uncertainty of about $10^{-2}\ M_\odot = 10\ M_{\rm Jup}$ ($M_{\rm Jup} \equiv$ Jupiter mass $\approx 10^{-3}\ M_\odot$) in this domain. Although not drastic for the present MF determinations, this uncertainty illustrates the level of accuracy to be reached eventually in the description of the physical properties of substellar objects, i.e., about a Jupiter mass, one-thousandth of a solar mass!

The lack of M-dwarf binary detection for the globular cluster or Galactic spheroid population prevents testing the MMRs for metal-depleted stellar abundances. A stringent observational constraint, however, stems from the observation of several cluster sequences down to the bottom of the MS with the *HST* cameras, in both the optical and the infrared domains. Globular clusters provide a special test to compare theory with observation since the metallicity, the distance, and the extinction are determined relatively accurately from the brightest stars, which leaves no free parameter to adjust the theory to observation. The Baraffe et al. (1997, hereafter BCAH97) models reproduce with excellent accuracy the observed sequences, in both optical and infrared colors, of clusters with metallicity ranging from [M/H] $= -2$ to [M/H] $= -1.0$ (Pulone et al. 1998; King et al. 1998; De Marchi, Paresce, & Pulone 2000; BCAH97), whereas the agreement near the bottom of the MS starts deteriorating in the optical for the more metal rich clusters ([M/H] > -1.0) (BCAH98; Bedin et al. 2001), as mentioned above for solar metallicity. As discussed at length in BCAH98, this shortcoming in the theory very likely stems from a missing opacity source in the optical, due to still incomplete treatment of metal/molecular line absorption. This shortcoming translates into theoretical sequences in optical colors that lie about 0.5 mag blueward of the observed sequences in M_V versus $V-I$ for metallicities [M/H] $\gtrsim -1.0$ (BCAH98; Fig. 1 of Chabrier et al. 2000a). This would affect appreciably the determination of the absolute magnitude of an object from its observed color, as occurs, for example, in the determination of the LF from photometric surveys, but as mentioned earlier, it affects only marginally the determination of a mass from an observed M_V magnitude. This uncertainty has been quantified in Chabrier (2001), who shows that the mass inferred from such a theoretical m-M_V relation is about 15% smaller than the one determined observationally by Delfosse et al. (2000). In terms of MF determination, this uncertainty remains within the observational Poisson error bars.

All these successful comparisons of theory with observation for low-mass stars and BDs, based on consistent evolutionary calculations between the emergent spectrum and the atmospheric and interior thermal profiles, i.e., consistent magnitude-color-mass-age relations, give us reasonable confidence in the MMR derived from these models and thus on the inferred MFs from observed LFs.

2. THE GALACTIC DISK MASS FUNCTION

2.1. The Field Mass Function

2.1.1. The Disk Stellar Luminosity Function

The determination of the low-mass star LF is a difficult task. First, the observed sample may be altered by various spurious effects: in a magnitude-limited sample, the so-called Malmquist bias leads to an overestimate of the local stellar space density. For surveys that reach large distances, corrections due to the Galactic structure should be taken into account; the exact completeness of the sample may be hard to determine with precision, in particular when estimating the BD space density. Last but not least, all surveys have limited angular resolution, so a certain fraction of the systems are unresolved. An extensive discussion of these various biases has been given in the papers by Kroupa, Tout, & Gilmore (1991, 1993) and Kroupa (1995).

The LF requires the determination of the distance of the objects. The easiest way to determine the distance is by knowing the trigonometric parallax, which implies a search within near distances from the Sun, typically $d \leq 20$ pc for the bright part of the LF ($M_V < 9.5$), which defines the Gliese Catalogue of Nearby Stars, a few parsecs for the faint end. For the faintest M dwarfs, the estimated completeness distance is $r_{\rm compl} \approx 5$ pc (Henry et al. 1997). This yields the so-called *nearby* LF $\Phi_{\rm near}$. The main caveat of the nearby LF is that, given the limited distance, it covers only a limited volume and thus a limited sample of objects. This yields important statistical indeterminations at faint magnitudes ($M_V \gtrsim 12$). On the other hand, a

fundamental advantage of the nearby LF, besides the reduced error on the distance and thus on the magnitude, is the accurate identification of binary systems. A *V*-band nearby LF can be derived by combining *Hipparcos* parallax data (ESA 1997), which are essentially complete for $M_V < 12$ at $r = 10$ pc, and the sample of nearby stars with ground-based parallaxes for $M_V > 12$ to a completeness distance $r = 5.2$ pc (Dahn et al. 1986). Henry & McCarthy (1990) used speckle interferometry to resolve companions of every known M dwarf within 5 pc and obtained the complete M-dwarf LF $\Phi_{\rm near}$ in the *H* and *K* bands. Their sample recovers the Dahn et al. (1986) one, plus one previously unresolved companion (GL 866B). Reid & Gizis (1997), and more recently Reid, Gizis, & Hawley (2002), extended this determination to a larger volume and determined a nearby LF based on a volume sample within about 8 pc. It turns out that, down to the limit of completeness claimed for the 8 pc sample, $M_V \sim 14$, the two LFs agree reasonably well.

Other determinations of the disk LF are based on photographic surveys, which extend to $d \approx 100$–200 pc from the Sun and thus encompass a significantly larger number of stars. However, photometric LFs $\Phi_{\rm phot}$ suffer in general from significant Malmquist bias, and as mentioned above, the low spatial resolution of photographic surveys does not allow the resolution of binaries at faint magnitudes. An extensive analysis of the different nearby and photometric LFs has been conducted by Kroupa (1995). As shown by this author, most of the discrepancy between photometric and nearby LFs for $M_V > 12$ results from Malmquist bias and unresolved binary systems in the low spatial resolution photographic surveys. (See also Reid & Gizis 1997 for an alternative point of view.) A recent determination of $\Phi_{\rm phot}$ was obtained with *HST* (Gould, Bahcall, & Flynn 1997, hereafter GBF97), which extends to an apparent magnitude $I \lesssim 24$. The Malmquist bias is negligible because all stars down to $\sim 0.1\ M_\odot$ are seen through to the edge of the thick disk. A major caveat of any photometric LF, however, is that the determination of the distance relies on a photometric determination from a color-magnitude diagram. The former analysis of the *HST* data (GBF97) used for the entire sample a color-magnitude transformation characteristic of stars with solar abundances. A significant fraction of the sample probed by *HST*, however, lies at a Galactic scale height $\| z \| \gtrsim 1$ kpc (Zheng et al. 2001, Fig. 2) and thus belongs to the thick-disk population and is likely to have metal-depleted abundances $-0.5 \lesssim$ [M/H] $\lesssim 0$. Assuming solar metallicity for the entire sample results in an underestimate of the absolute magnitude for a given color (the lower the metallicity, the fainter the absolute magnitude for a given color) and thus an overestimate of the distance and an underestimate of the number density, in particular near the faint end of the LF. An extension and a reanalysis of the *HST* sample, taking into account a statistically weighted metallicity gradient along the Galactic scale height and a related color-magnitude-metallicity relationship, yield a revised Φ_{HST} (Zheng et al. 2001), with indeed a larger number of M dwarfs at faint absolute magnitude. However, because of its limited angular resolution (<0″.1), *HST* misses all the binaries, and the LF must be corrected from this caveat to yield a single LF (§ 2.1.3 below).

In practice, the determination of the MF from the LF implies the knowledge of each star's chemical composition, since the colors and the magnitude depend on the metallicity. This metallicity spread translates into a spread in the LF and in the MF. Analysis of the *Hipparcos* color-magnitude diagram, however, indicates that ~90% of the thin-disk stars have abundances [M/H] $= 0 \pm 0.2$ (Reid 1999), so the spread of metallicity in the solar neighborhood should not affect significantly the derivation of the MF through the MMR.

The magnitude of an object, however, varies with age, so the determination of its mass through a theoretical MMR necessitates the knowledge of its age. The luminosity of MS stars above $m \sim 0.7\ M_\odot$ starts increasing substantially after ~10 Gyr, about the age of the Galactic disk. On the other hand, objects below $m \sim 0.13\ M_\odot$ (for a solar composition) take more than 5×10^8 yr to reach the main sequence (see Table 1 of Chabrier & Baraffe 2000). Therefore, for a constant SFR and a age of the disk $\tau_D = 10$ Gyr, at most ~5% of the nearby stars in the mass range $0.13 \leq m/M_\odot \leq 0.7$ might still be contracting on the pre–main sequence (PMS), an uncertainty well within the statistical observational ones. Within this mass range, the position of the star is fixed in the mass-luminosity diagram. Below $0.1\ M_\odot$, and in particular in the BD domain, age variations must be taken into account, within a given SFR, for a proper determination of the MF from the observed star or BD counts (Chabrier 2002).

2.1.2. The Disk Stellar Mass Function

Recently, Chabrier (2001) has determined the Galactic disk M-dwarf MF from the 5 and 8 pc $\Phi_{\rm near}$. He has shown that, although still rising down to the H-burning limit, the IMF $\xi(\log m)$ starts becoming shallower than the Scalo or Salpeter value below $\sim 1\ M_\odot$ and flattens out below $\sim 0.3\ M_\odot$, as noted previously by MS79 and Kroupa et al. (1993). Combining the M-dwarf MF with the Scalo (1986) power law for masses above $1\ M_\odot$, and fulfilling the so-called continuity condition for stars with $\tau_{\rm TO} \approx \tau_{\rm G}$ (MS79), i.e., $m \simeq 0.9\ M_\odot$, Chabrier (2001) showed that the MF is well described over the entire stellar mass range from about 100 to $0.1\ M_\odot$ by any of the functional forms mentioned in § 1.2.3, i.e., a two-segment power law, a lognormal form, or an exponential (Rosin-Rammler) form. This analysis has been completed by Chabrier (2003), who has calculated the MF from the nearby LF $\Phi_{\rm near}$ obtained both in the *V* band (Dahn et al. 1986) and in the *K* band (Henry & McCarthy 1990). Figure 1 displays such a comparison. The conversion of the *V*-band LF into an MF was done using the Delfosse et al. (2000) m-M_V relation, which fits the observed data, whereas the BCAH98 m-M_K relation was used to convert the *K*-band LF. We note the very good agreement between the two determinations, which establishes the con-

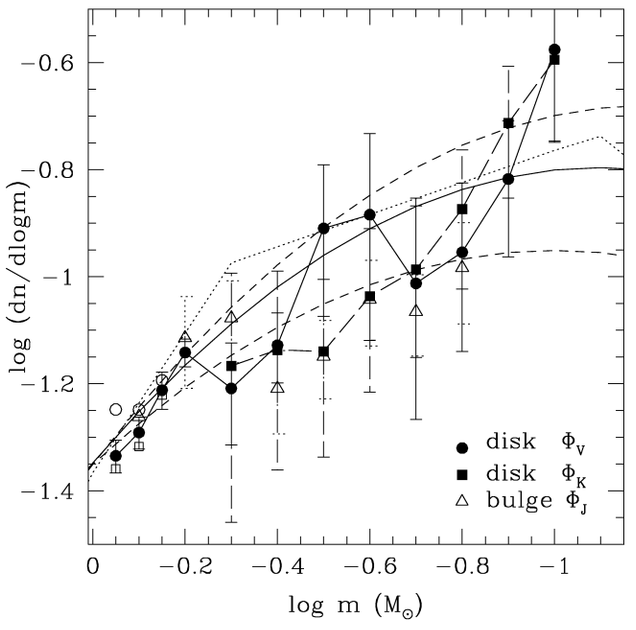

FIG. 1.—Disk mass function derived from the local *V*-band LF (*circles and solid line*) and *K*-band LF (*squares and dashed line*). The solid line and the two surrounding dashed lines display the lognormal form given by eq. (17), whereas the dotted line illustrates the four-segment power-law form of Kroupa (2002). The open circles and squares for $\log m \geq -0.15$ display the MF obtained for $t = 10$ and 1 Gyr, respectively, illustrating the age uncertainty on the MF for $m > 0.7\ M_\odot$. The open triangles and dotted error bars display the MF obtained from the bulge LF (see text).

sistency of the two observed samples and the validity of the mass-magnitude relationships. The ~1.5 σ difference in the mass range $\log m \sim -0.5$ to -0.6, i.e., $M_V \sim 12$–13, reflects the remaining uncertainties either in the MMR or in the LF $\Phi_{\rm near}$. The MF derived from the new *V*-band LF of Reid et al. (2002), not displayed in Figure 1, closely resembles the one derived from the Henry & McCarthy (1990) *K*-band LF. The solid line displays an analytic form that gives a fairly good representation of the results. The uncertainties in the MF are illustrated by the surrounding dashed lines. This analytic form for the disk MF for single objects below 1 $M_\odot$, within these uncertainties, is given by the following lognormal form (Chabrier 2003):

$$\xi(\log m)_{m\leq 1} = 0.158^{+0.051}_{-0.046} \times \exp\left\{-\frac{(\log m - \log 0.079^{-0.016}_{+0.021})^2}{2 \times (0.69^{-0.01}_{+0.05})^2}\right\} (\log M_\odot)^{-1}\ \mathrm{pc}^{-3}. \quad (17)$$

The derivation of this MF from the *Hipparcos* and local sample provides a normalization at 0.7 $M_\odot$ of $(dn/dm)_{0.7} = 3.8 \times 10^{-2}\ M_\odot^{-1}\ \mathrm{pc}^{-3}$, with at most a 5% uncertainty. Age effects above 0.7 $M_\odot$ are illustrated in the figure by the open circles and open squares, which display the MF obtained with the MMR for $t = 10$ and 1 Gyr, respectively, whereas the filled circles correspond to $t = 5$ Gyr, the average age for the Galactic thin disk.[4] As mentioned previously, age effects become negligible below $m = 0.7\ M_\odot$. The dotted line displays part of the four-segment power-law MF derived by Kroupa (2002). This MF slightly overestimates the M-dwarf density.

TABLE 1
DISK IMF AND PDMF FOR SINGLE OBJECTS

Parameter	IMF	PDMF
$m \leq 1.0\ M_\odot$, $\xi(\log m) = A \exp[-(\log m - \log m_c)^2/2\sigma^2]$		
A	$0.158^{+0.051}_{-0.046}$	$0.158^{+0.051}_{-0.046}$
m_c	$0.079^{-0.016}_{+0.021}$	$0.079^{-0.016}_{+0.021}$
σ	$0.69^{-0.01}_{+0.05}$	$0.69^{-0.01}_{+0.05}$
$m > 1.0\ M_\odot$, $\xi(\log m) = Am^{-x}$		
A	4.43×10^{-2}	
x	1.3 ± 0.3	
$0 \leq \log m \leq 0.54$:		
A		4.4×10^{-2}
x		4.37
$0.54 \leq \log m \leq 1.26$:		
A		1.5×10^{-2}
x		3.53
$1.26 \leq \log m \leq 1.80$:		
A		2.5×10^{-4}
x		2.11

NOTE.—For unresolved binary systems, the coefficients are given by eq. (18). The normalization coefficient A is in $(\log M_\odot)^{-1}\ \mathrm{pc}^{-3}$.

Note that equation (17) yields the Scalo (1986) normalization for 5 Gyr at 1 $M_\odot$, $(dn/dm)_{1.0} = 1.9 \times 10^{-2}\ M_\odot^{-1}\ \mathrm{pc}^{-3}$, which corresponds to a condition $M_V = 4.72$ for $m = 1.0\ M_\odot$ at 5 Gyr. As shown by Scalo (1986) and illustrated in Figure 1, 1 $M_\odot$ is about the limit at which the disk PDMF and IMF start to differ appreciably, so that only the $m > 1\ M_\odot$ power-law part of the MF will differ, depending on whether the IMF ($x = 1.3 \pm 0.3$) or the PDMF (x given by eq. [11]) is considered. This yields the global disk PDMF and IMF, as summarized in Table 1. As mentioned earlier, substantial uncertainty remains in the value of x at large masses for the IMF. As will be discussed in § 7, observations of high-z galaxies, which constrain the fraction of very massive stars to solar-type stars, seem to favor a Salpeter slope at large masses and to exclude a Scalo slope. For these reasons, we elected to take a Salpeter exponent for the IMF above 1 $M_\odot$, with the aforementioned ~0.3 uncertainty.

As shown by Chabrier (2001) and Kroupa (2001), the low-mass part of the MF can be described by a one- or two-segment power law. Extension of these segments into the BD domain, however, severely overestimates the number of BD detections

[4] The vast majority of stars in the Galactic midplane belong to the old disk ($h \sim 300$ pc, $\tau \sim 5$ Gyr) and about 20% to the young disk ($h \sim 100$ pc, $\tau \sim 1$ Gyr) (see, e.g., Gilmore & Reid 1983).

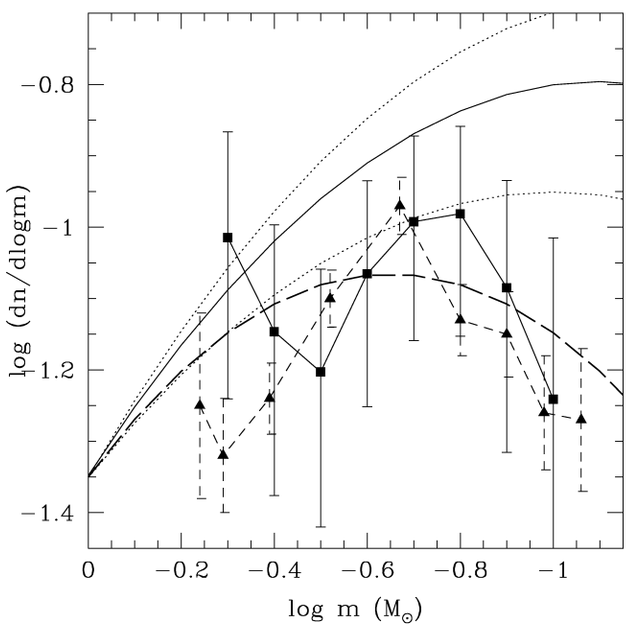

FIG. 2.—Disk mass function derived from the system *K*-band LF (*filled squares and solid line*) and the *HST* corrected MF (*triangles and short-dashed line*) from Zheng et al. (2001). The solid line and surrounding dotted lines display the lognormal form given by eq. (17) for single objects, as in Fig. 1, whereas the dashed line illustrates the lognormal form given by eq. (18).

(Chabrier 2002), thus requiring another, different power-law segment in this regime. Such many-segment power-law functions, implying as many characteristic masses, seem difficult to reconcile with reasonable scenarios of star formation. A power law at large masses and a lognormal form in the low-mass range, implying one single characteristic mass, on the other hand, seems to be supported by physically motivated scenarios, as will be discussed in § 7. For this reason, the PDMF and IMF displayed in Table 1 seem to be favored over other functional forms.

Figure 1 also displays the IMF derived from the observed *J*-band LF of the Galactic bulge (Zoccali et al. 2000) down to its completeness limit ($J \sim 24$, $M_J \sim 9$, $m \sim 0.15\ M_\odot$) with the BCAH98 MMR, for an age 10 Gyr and a solar metallicity (*open triangles*). The bulge IMF is normalized to the disk value at 0.7 $M_\odot$. We note the remarkable agreement between the bulge and the disk IMF.

2.1.3. Correction for Binaries: The Disk System Mass Function

As demonstrated by the detailed study of Kroupa et al. (1991, 1993), correction for unresolved binaries can lead to a major revision of the IMF below about 1 $M_\odot$. This study demonstrated that part of the disagreements between photometric and parallax surveys stemmed from unresolved binaries and Malmquist bias. The disagreement between the MF inferred from the aforementioned nearby LF and from the photometric *HST* LF (GBF97), however, had remained a controversial, unsettled issue until recently (see, e.g., Fig. 1 of Méra, Chabrier, & Schaeffer 1998). As mentioned in § 2.1.1, an important source of the disagreement was the assumption by GBF97 of a solar composition for the stars in the *HST* sample for the photometric determination of the distance. This yields an underestimate of the faint part of the LF, as demonstrated in Figure 4 of Zheng et al. (2001). The other source of discrepancy was the contribution from unresolved binaries in the *HST* LF. Indeed, as mentioned earlier, because of its angular resolution, *HST* resolves only ~1% of the multiple systems (see GBF97). Since about half of the stars are known to be in multiple systems, the *HST* LF misses essentially all companions. Recently, Chabrier (2003) has conducted a detailed analysis of the bias due to unresolved binaries with the new (Zheng et al. 2001) *HST* LF. This author has shown that the MF derived from the revised *HST* LF (1) is very similar to the local so-called *system* MF, i.e., the MF derived from the local LF once the companions of all identified multiple systems have been merged into unresolved systems; and (2) is consistent with the single MF (eq. [17]) providing a binary fraction $X \approx 50\%$ among M dwarfs, with the mass of both the single objects and the companions originating from the same single MF (eq. [17]). This multiplicity rate implies that about ~30% of M dwarfs have a *stellar* (M dwarf) companion, whereas about ~20% have a *substellar* (BD) companion (Chabrier 2003), a result in agreement with present-day determinations of the M-dwarf binary fraction in the solar neighborhood (Marchal et al. 2003) and of BD companions of M dwarfs (Gizis et al. 2001; Close et al. 2003). This system MF can be parameterized by the same type of lognormal form as the single MF (eq. [17]), with the same normalization at 1 $M_\odot$, with the coefficients (Chabrier 2003)

$$\xi(\log m)_{m\leq 1} = 0.086 \exp\left[-\frac{(\log m - \log 0.22)^2}{2 \times 0.57^2}\right] (\log M_\odot)^{-1}\ \mathrm{pc}^{-3} \qquad (18)$$

and is displayed by the long-dashed line in Figure 2.

These calculations show that the disk stellar IMFs determined from either the nearby geometric (parallax) LF or the *HST* photometric LF are consistent and that the previous source of disagreement was due to *two effects*, namely, (1) incorrect color-magnitude determined parallaxes, because a substantial fraction of the *HST* M-dwarf sample belongs to the metal-depleted, thick-disk population, and (2) unresolved binaries. As discussed in Chabrier (2003), these results yield a reinterpretation of the so-called brown dwarf desert. The latter expresses the lack of BD companions to solar-type stars (G–K), as compared with stellar or planetary companions, at separations of less than 5 AU (Marcy, Cochran, & Mayor 2000). Indeed, proper motion data from *Hipparcos* have revealed that a significant fraction of low-mass companions in the substellar regime have low inclination and thus larger, possibly stellar masses (Marcy et al. 2000; Halbwachs et al. 2000). Correction

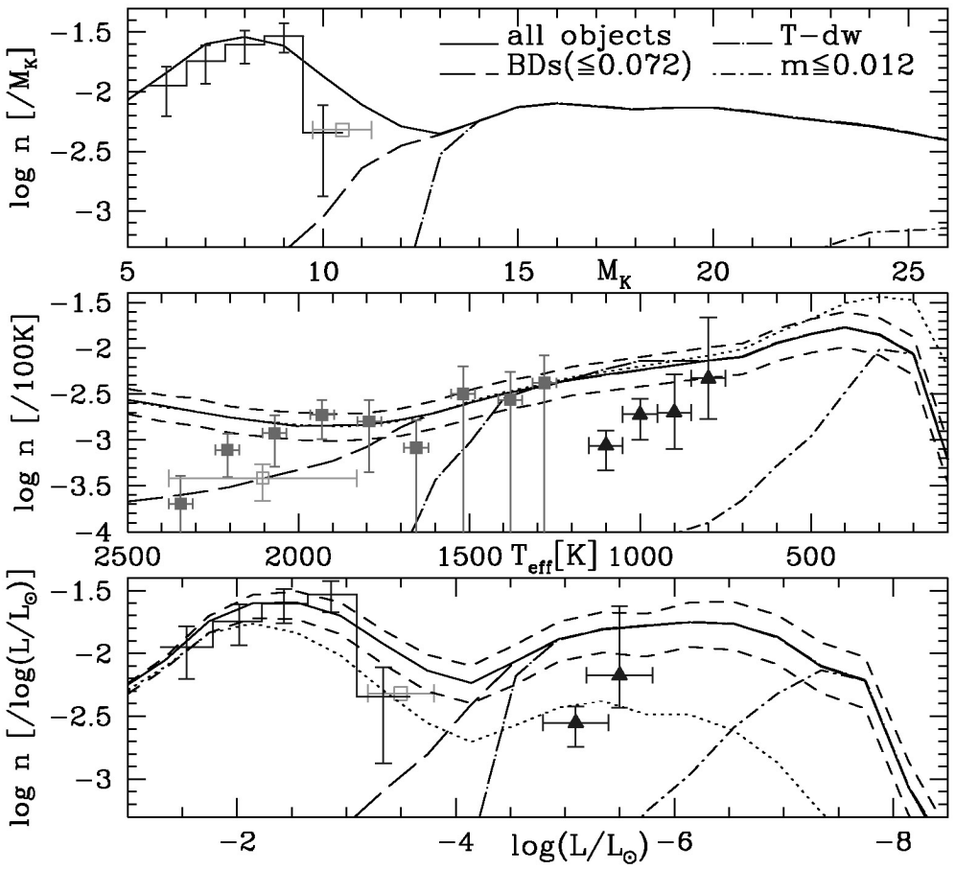

FIG. 3.—Luminosity functions for the Galactic disk predicted with the IMF (eq. [17]) and a constant SFR. *Solid line:* stars+BDs; *long-dashed line:* BDs only ($m \leq 0.072\ M_\odot$); *long-dash–dotted line:* T dwarfs only ($J-H < 0.5$ and $H-K < 0.5$); *short-dash–dotted line:* objects below the D-burning minimum mass ($m \leq 0.012\ M_\odot$). The short-dashed lines illustrate the range of uncertainty in the IMF (eq. [17]). The dotted line in the middle panel displays the result obtained with a power-law IMF with $x = 0$ [$\xi(\log m) \propto$ constant] with the same normalization at $0.1\ M_\odot$ as the IMF (eq. [17]). The dotted line in the bottom panel displays the results obtained with the system IMF (eq. [18]). The histogram displays the nearby LF (Henry & McCarthy 1990). Open and filled squares are estimated L-dwarf densities by Gizis et al. (2000) and Kirkpatrick et al. (1999, 2000)+Burgasser (2001), respectively. Triangles are estimated T-dwarf densities from Burgasser (2001).

for this inclination yields a deficit of small-separation BD companions, the BD desert, suggesting that the MF of substellar companions to solar-type stars, at least at separations less than 5 AU, differs significantly from the one determined for the field. The present calculations, however, show that this "desert" should be reinterpreted as a lack of high mass ratio ($q = m_2/m_1 \lesssim 0.1$) systems and does not preclude a substantial fraction of BDs as companions of M dwarfs or other BDs, as suggested by recent analysis (Marchal et al. 2003; Burgasser et al. 2003; Close et al. 2003).

2.1.4. Disk Brown Dwarf Mass Function

As shown in § 2.1.2, the IMF (eq. [17]) gives a good representation of the stellar regime in the disk down to $\log m \sim -0.9$ ($m \sim 0.12\ M_\odot$), where all objects have reached the MS. This IMF, which closely resembles the IMF2 derived in Chabrier (2001), gives also a good description of the star counts in the deep field of the ESO Imaging Survey (EIS; Groenewegen et al. 2002), better than the power-law forms of Kroupa (2001) or IMF1 of Chabrier (2001). It has been shown also to agree fairly well with the L-dwarf and T-dwarf BD detections of various field surveys (Chabrier 2002). Figure 3 displays the predicted BD luminosity functions (BDLF) in the K magnitude and in terms of fundamental parameters ($T_{\rm eff}$, $L/L_\odot$) from the bottom of the MS over the entire BD domain. These BDLFs were obtained from Monte Carlo simulations, with mass, age, and distance probability distributions as described in Chabrier (2002). Only the case of a constant SFR has been considered presently. The various dashed and dotted lines display the relative contributions of BDs ($m \leq 0.072\ M_\odot$ for solar metallicity; Chabrier & Baraffe 1997); T dwarfs, identified as faint objects with $J-H < 0.5$, $H-K < 0.5$ (Kirkpatrick et al. 2000); and objects below the deuterium-burning limit ($m \leq 0.012\ M_\odot$). The predictions are compared with various available data, namely,

the nearby *K*-band LF (Henry & McCarthy 1990), converted into a bolometric LF in the bottom panel with the M-dwarf bolometric corrections of Tinney, Mould, & Reid (1993) and Leggett et al. (1996); the L-dwarf density estimate of Gizis et al. (2000); and the L-dwarf and T-dwarf estimated densities of Kirkpatrick et al. (1999, 2000) and Burgasser (2001). It is important to mention that the $V_{\rm max}$ and thus the explored volume and density determinations for BD surveys are a very delicate task, affected by numerous uncertainties (see Burgasser 2001). An ~1 mag uncertainty in the maximum limit of detection translates into a factor of ~4 in $V_{\rm max}$ and thus in the estimated density $\Phi = \Sigma V_{\rm max}^{-1}$, not to mention difficult completeness corrections for such surveys. Furthermore, the observational $T_{\rm eff}$ and bolometric correction determinations are presently ill determined for BDs. On the other hand, theoretical models of BD cooling, although now in a mature state, are still far from including all complex processes such as dust sedimentation, cloud diffusion, or nonequilibrium chemistry. For all these reasons, the present results should be considered with caution. The BDLFs calculated with the IMF (eq. [17]) yield a very good agreement with the determinations of Kirkpatrick et al. (1999, 2000) but seem to overestimate by a factor of about 3 the density of L dwarfs obtained by Gizis et al. (2000) and the number of bright T dwarfs observed by Burgasser (2001). The decreasing number of L dwarfs in the Kirkpatrick et al. (1999) survey at bright magnitudes is due to their color selection ($J-K > 1.3$). Given all the aforementioned uncertainties, the comparison between the observed and predicted LFs can be considered as satisfactory. This assesses the validity of the present disk IMF determination in the BD regime.

The factor of ~3 overestimate of the predicted LF, if confirmed, might stem from various plausible explanations. First, this might indicate too high a normalization of the IMF near the bottom of the MS, due to the presence of hot BDs misidentified as MS very low mass stars in the faintest bins of the nearby LF. However, as seen from the top panel of Figure 3, the contribution of young BDs to the local LF is zero for $M_K \leq 9$, which corresponds to an ~0.12 $M_\odot$ MS M dwarf and thus does not affect the MF normalization at this mass. An alternative, similar explanation would be the presence of a statistically significant number of very low mass stars younger than 10^8 yr, still contracting on the PMS, in the local sample. This implies a small scale height for these objects. Indeed, for a constant SFR and a young-disk age $\tau \simeq 1$ Gyr, the probability of finding an object with $t < 10^8$ yr is ~10% for a homogeneous sample. Only redoing the same observations in a few hundred million years could help resolving this issue, a rather challenging task! A second possible explanation could be unresolved BD binaries. The dotted line in the bottom panel of Figure 3 displays the LF obtained with the IMF (eq. [18]), illustrating the effect due to BD unresolved systems. The effect of unresolved binaries on the BDLF is much more dramatic than on the stellar LF. This stems from the much steeper mass-magnitude relationship at a given age in the BD regime. At 1 Gyr, a factor of 2 in mass corresponds to about ~2 mag difference in the stellar regime, against ~4 mag or more in the BD regime. On the other hand, remember that the difference between the single (eq. [17]) and system (eq. [18]) MFs assumes a binary correction $X \approx 50\%$ among *stellar* objects. Extrapolating these corrections into the BD domain assumes that the binary rate in star formation does not depend on the mass of the primary. If the present discrepancy between theory and observation is confirmed, it might indicate that this frequency is significantly smaller in the BD regime (with $X \lesssim 20\%$) because, for example, very low mass systems cannot form with large mass ratios ($q = m_2/m_1 \ll 1$) or with large orbital separations (see, e.g., Burgasser et al. 2003).[5] Again, long time basis observations are mandatory to nail down this issue. A third, appealing explanation for the factor of 3 discrepancy might be substantial incompleteness of the present BD surveys resulting from selection effects. Salim et al. (2003) estimate that some 40% of bright L dwarfs are missed because they lie close to the Galactic plane, a region avoided by most searches. This correction factor would bring the present theoretical predictions in perfect agreement with the observational BD census. Finally, the present factor of ~3 disagreement between the predicted and observationally derived counts might just reflect the remaining imperfections in BD cooling models.

It is interesting to note the bimodal form of the stellar+BD LFs. The stellar LF peaks near the bottom of the MF because of the rising IMF. The LF then decreases severely because of the steepness of the MMR below ~0.2 $M_\odot$, where a very small mass range translates into a large magnitude interval, a consequence of the decreasing nuclear support to halt contraction (Chabrier & Baraffe 1997, 2000). The brightest, i.e., youngest and most massive BDs start contributing near $\log (L/L_\odot) \simeq -3$, but the bulk of the BD population dominates the LF only ~1.5 mag fainter. The BDLF thus rises again, a direct consequence of the cumulative effects of the increasing number of BDs and of BD cooling. The decreasing IMF eventually yields decreasing BD densities for $\log (L/L_\odot) \lesssim -6$, $T_{\rm eff} \lesssim 400$ K. The observational confirmation of the dip in the BDLF near $\log (L/L_\odot) \simeq -4$, $M_K \simeq 13$ would be an interesting confirmation of the present general theory (IMF and BD cooling). The dotted line in the middle panel of Figure 3 displays the results obtained with a power-law MF $\xi(\log m) = m^x$ with $x = 0$ ($\alpha = 1$) for the same normalization as the IMF (eq. [17]) at 0.1 $M_\odot$. As already noted by Chabrier (2002), such an MF yields very similar results in the L-dwarf and hot T-dwarf range but predicts more cool T dwarfs. Note that the same power-law MF ($x = 0$), but with a normalization $\xi(\log m = -1) = 0.08\ (\log M_\odot)^{-1}\ {\rm pc}^{-3}$, as in Reid et al. (1999), instead of $0.156\ (\log M_\odot)^{-1}\ {\rm pc}^{-3}$ (eq. [17]), would bring predicted and observationally derived LFs in very good agreement. Such a

[5] Note that the BD binaries observed by Burgasser et al. (2003) have an orbital separation greater than 1 AU and do not include BD systems with smaller separation such as PPL 15.

low normalization near the bottom of the MS, however, is likely due to the incompleteness of the 8 pc sample at faint magnitudes, as can be seen easily from a comparison of the Reid & Gizis (1997) revised *K*-band LF and the Henry & McCarthy (1990) one (displayed at the top of Fig. 3; see also Chabrier 2001, Fig. 2).

2.2. The Young Cluster Mass Function

In principle, star-forming regions (age $\lesssim$1 Myr, e.g., ρ Oph, IC 348, Trapezium, Taurus-Auriga, Chameleon I, Serpens) or young clusters (age ~10–200 Myr, e.g., Pleiades) are particularly favorable targets to determine the very initial stellar mass function. Indeed, (1) all objects in the cluster are likely to be coeval within a limited range, except possibly in star-forming regions, where the spread in ages for cluster members can be comparable with the age of the cluster; (2) young objects are brighter for a given mass, which makes the detection of very low mass objects easier; (3) young clusters are less dynamically evolved than older open clusters and thus subtend a more compact region of the sky, yielding smaller foreground and background contamination. In practice, however, the determination of the IMF is hampered by several difficulties from both the observational and theoretical sides. First, membership of the objects to the cluster must be assessed unambiguously, which implies either accurate spectroscopic observations (lithium absorption, Hα emission, millimeter excess, etc.) for the regions of star formation or accurate proper-motion measurements for the young clusters. Second, extinction and differential reddening caused by the surrounding dust in star-forming regions modify both the intrinsic magnitude and the colors of each individual object, preventing direct mass-magnitude-color determinations and making photometric determinations very uncertain, not to mention the amount of accretion, which varies significantly from one object to another (see, e.g., Comerón et al. 2003). Moreover, the near-IR excess of embedded young clusters associated with hot circumstellar dusty disks complicates significantly the interpretation of near-IR luminosity into *stellar* luminosity functions. Third, *some* dynamical evaporation may have taken place, rejecting low-mass objects to the periphery of the cluster, where contamination from field stars become important. This holds even for very young clusters (<1 Myr) that contain O stars, such as, e.g., the Orion Nebula cluster (Kroupa, Aarseth, & Hurley 2001). Finally, there is presently no appropriate effective temperature calibration for gravities characteristic of PMS M dwarfs, causing researchers to rely on empirical $T_{\rm eff}$–spectral type (Sp) determinations, as discussed below.

From the theoretical point of view, accurate models must include gravity effects, which, for young objects, affect both the spectrum and the evolution (Baraffe et al. 2002). As shown by these authors, *no* theoretical model is presently reliable for ages younger than ~10^6 yr. At such young ages, the evolution is severely affected by several uncertainties, e.g., the unknown convection efficiency (and thus mixing-length parameter), the accretion rate, and the deuterium abundance, not to mention the fact that at these ages the models are affected by the (arbitrary) initial conditions. As shown by Baraffe et al. (2002), the evolution along the contracting PMS phase for $t \lesssim 10^6$ yr depends not only on the (unknown) efficiency of convection but also, for the coolest objects, on the formation of molecular hydrogen H_2 in the atmosphere. Both effects significantly affect the evolution. Therefore, assuming a constant $T_{\rm eff}$ evolution for a given mass in an HR diagram for young, very low mass objects, as sometimes done in the literature, may lead to inaccurate mass determinations, and the inferred IMFs must be considered with great caution. In fact, three-dimensional calculations are necessary to determine accurately the entropy profile of objects in the initial accreting, gravitational contracting phase, for one-dimensional collapse calculations yield erroneous results (Hartmann, Cassen, & Kenyon 1997; Hartmann 2003; Baraffe et al. 2003). No such consistent calculation and thus no reliable temperature and mass calibration exists today for low-mass PMS stars. Only for ages $t \gtrsim 10^6$ yr do these uncertainties disappear, or at least become less important, and can reasonably reliable PMS models be calculated (Baraffe et al. 2002). Finally, as pointed out by Luhman et al. (2000), what is really observed in star-forming clusters is not the IMF but the creation function (see § 1.2.2). The same underlying IMF convolved with different age distributions will yield different LFs, a result that can be misinterpreted as originating from different IMFs. Conversely, assuming a single, median age for objects in star-forming regions, where the typical age spread can reach a few Myr, yields an IMF of limited validity, given the strong age dependence of the mass-luminosity relationship for PMS and young stars. Without an independent estimate of the age distribution of the cluster members, the creation function and thus the IMF cannot really be determined, not to mention the fact that no one knows whether the star-forming process in the star-forming regions or very young clusters is finished or is still going on and thus whether the mass function is really the *initial* mass function. For all these theoretical and observational reasons, the exact determination of the IMF of star-forming regions or very young ($\lesssim 10^6$ yr) clusters remains presently speculative, and IMF determinations claimed so far in the literature are of limited significance. Only general features, such as ratios of substellar over stellar objects, can be considered as reasonably reliable indicators. On the other hand, star-forming regions are certainly very useful testbeds to study the various processes of star formation (accretion, multiplicity, collisions, rotation, etc.).

As mentioned above, no accurate $T_{\rm eff}$ calibration exists today for PMS low-mass stars. However, an interesting, although empirical, method has been suggested by Luhman (1999), based on the analysis of the GG Tau system by White et al. (1999), to calibrate the effective temperature from the spectral type of young low-mass stars. Since such objects have gravities between M giants and M dwarfs, Luhman (1999) derived a

$T_{\rm eff}$-Sp relation intermediate between those of giants and dwarfs, based on the 6500–9000 Å observed spectra. When using this relationship, the four components of the quadruple system GG Tau, which extend from 1.2 to about 0.03 $M_\odot$, lie on a common isochrone of the BCAH98 models, for the correct, dynamically determined mass of the system. Luhman (1999) further showed that the spectra of PMS stars in IC 348 are better fitted by an average of dwarf and giant spectra of the same spectral type, and the combination of BCAH98 isochrones and Luhman's (1999) $T_{\rm eff}$ scale provides the best fit to the IC 348 cluster locus (Luhman 1999; Najita, Tiede, & Carr 2000). However, one must remains cautious with such an agreement, which could happen to be coincidental, and with the aforementioned empirical $T_{\rm eff}$-Sp relation. As noted by Najita et al. (2000), the latter does not apply at cool temperatures in spectral regions shaped by water-band absorption in the infrared because of the dissociation of water due to the back-warming effect, which yields eventually a *cooler* temperature scale for M-dwarf PMS gravities below 3000 K. Moreover, this intermediate $T_{\rm eff}$-Sp relationship is approximated by a simple linear fit. Such a linear dependence between spectral type and effective temperature is unlikely to be adequate over a large range of spectral types.

Keeping all these limitations in mind, the results of Luhman et al. (2000) point to an interesting suggestion. Using the aforementioned $T_{\rm eff}$-Sp relationship, i.e., a consistent methodology for the analysis of various observations, these authors derived what is supposed to be the IMF of several star-forming clusters, namely, IC 348, ρ Oph, or the Trapezium, and showed that these IMFs are very similar, except for the Taurus star-forming region, which exhibits a significant deficit of BDs, as confirmed recently by the larger survey of Briceño et al. (2002). Although, as mentioned earlier, these MF determinations, in spite of the effort of these authors, are of limited reliability, given the very young age of these clusters (<1 Myr), they seem to indicate a (moderately) rising MF in the substellar regime down to about the deuterium-burning limit. This is confirmed by Najita et al. (2000), who conducted a very careful study of IC 348 in the infrared with *HST* extending 4 mag below the previous *K*-band study of Luhman (1999). Using BCAH98 models and the Luhman (1999) temperature scale, these authors obtain an MF $\xi(\log m) \propto m^{0.5}$ in the mass range $0.015 \lesssim m/M_\odot \lesssim 0.7$, based on the four lowest mass bins of the sample.

More robust determinations can be derived from the observations of older, so-called young open clusters such as the Pleiades ($\tau \approx 100$ Myr). Figure 4 displays the MF obtained for the Pleiades from various observed LFs covering a significant fraction of the cluster area (Hambly et al. 1999; Dobbie et al. 2002b; Moraux et al. 2003), using the BCAH98 and Chabrier et al. (2000a) models, which accurately reproduce the observed magnitude-color diagrams. Membership in the cluster has been assessed by proper motion measurements and follow-up observations in the near-IR. The field single-object IMF (eq. [17]) and system IMF (eq. [18]) derived in § 2.1 are displayed for comparison (*dashed lines*). As seen in the figure, the MF derived from the observed LF is adequately reproduced by the disk *system* MF (eq. [18]), suggesting that the difference between the Pleiades MF and the field single MF stems primarily from unresolved companions, assuming the same kind of correction for binaries as for the field, and possibly from a moderate dynamical evaporation of very low mass objects (see also Moraux et al. 2003).[6]

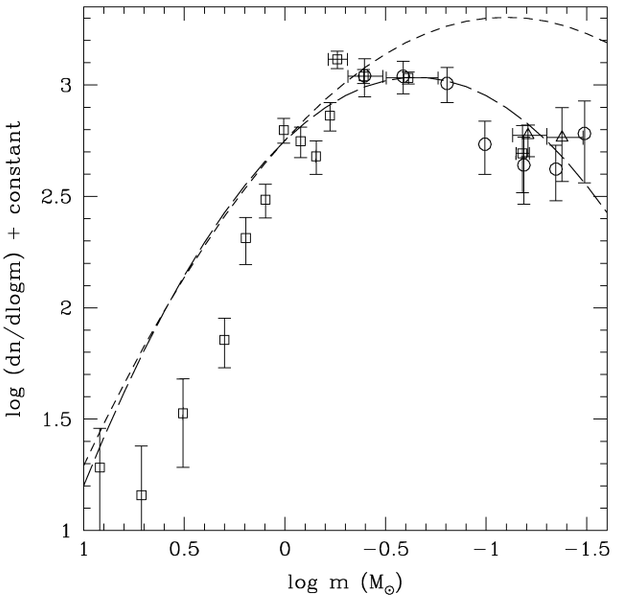

FIG. 4.—Pleiades mass function calculated with the BCAH98 and Chabrier et al. (2000a) MMRs from various observations. *Squares:* Hambly et al. (1999); *triangles:* Dobbie et al. (2002b); *circles:* Moraux et al. (2003). The short-dashed and long-dashed lines display the single (eq. [17]) and system (eq. [18]) field MFs, respectively, arbitrarily normalized to the present data.

Figure 5 displays the MFs obtained for various similar clusters, with ages ranging from ~5 to ~170 Myr. Again, membership of the very low mass objects in the clusters has been assessed by accurate proper-motion measurements (better than 10 mas yr^{-1}) or by follow-up spectroscopy (see references in the figure legend). The σ Orionis cluster, in spite of its relatively young age, exhibits negligible extinction (Zapatero Osorio et al. 2000), and masses can be inferred from MMRs at the proper age. It is important to note that these observations do not consider the effect of binarity, so the derived MFs reflect the system MFs. The field system MF (eq. [18]) is superposed for each cluster for comparison (*long-dashed lines*). We verified that this system MF also reproduces very well the MF derived for the young cluster IC 348 (Luhman et al. 2003) down to ~0.01 $M_\odot$.

Figure 5 clearly points to a similar underlying IMF between

[6] The difference between the observed and theoretical MF at large masses stems from incompleteness in the Hambly et al. (1999) survey, completed recently by Adams et al. (2001).

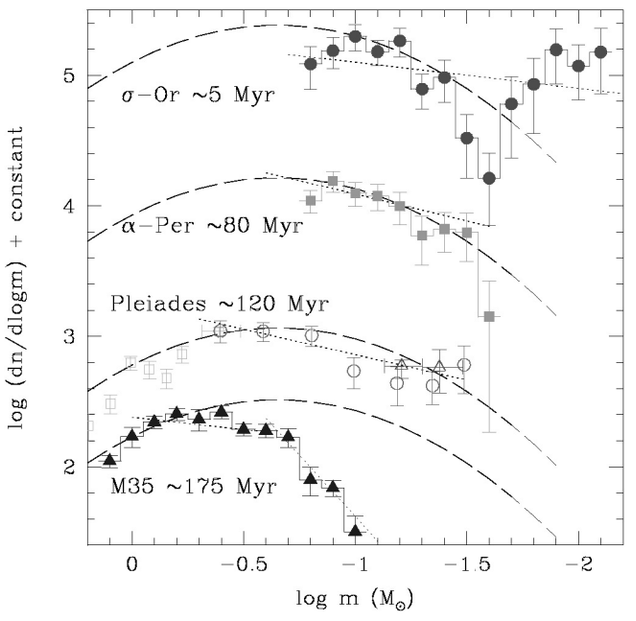

FIG. 5.—Mass function calculated for various young clusters with the BCAH98 and Chabrier et al. (2000a) MMRs, from various data. *Filled circles:* σ Ori (Béjar et al. 2001); *filled squares:* α Per (Barrado y Navascues et al. 2002); *filled triangles:* M35 (Barrado y Navascues et al. 2002). Open symbols are for the Pleiades (*squares:* Hambly et al. 1999; *circles:* Moraux et al. 2003; *triangles:* Dobbie et al. 2002b). The ages for each cluster are indicated. The dashed line illustrates the field system MF (eq. [18]), while the dotted lines display various power-law segments $\xi(m) = dN/d\log m \propto m^{-x}$, as derived by the aforementioned authors, with $x = -0.2$ (σ Ori), $x = -0.4$ (α Per), $x = -0.4$ (Pleiades), and $x = -0.2$ and -1.9 (M35).

open clusters and the Galactic field, extending below the H-burning limit. Differences are likely to arise from unresolved binaries and from uncertainties in the mass determination of the lowest mass objects, due to uncertainties in the theoretical models at young ages (see Baraffe et al. 2002) and in the treatment of dust formation (Chabrier et al. 2000a and discussion in § 1.3). The same figure also illustrates the effect of dynamical evolution, which affects predominantly the lowest mass objects. As suggested by the present analysis, dynamical evolution starts to significantly affect the IMF of the clusters somewhere between the ages of the Pleiades (~120 Myr) and the age of M35 (~175) Myr. This estimate is in agreement with recent *N*-body star cluster simulations, which predict very limited evaporation ($\lesssim$10%) within 100 Myr (de la Fuente Marcos & de la Fuente Marcos 2000). It is thus not surprising that deep surveys of the Hyades (~800 Myr) have failed to discover any BDs (Gizis, Reid, & Monet 1999; Dobbie et al. 2002a). These results corroborate the traditional view that the Galactic field has been populated from the evaporation of young, dense ($n \gtrsim 10^3$ pc^{-3}) clusters as the one considered presently, with the same underlying IMF.

The amount of evaporation of a cluster and thus the departure from the IMF can be determined by the approximate number of objects and total mass in a mass range domain relative to a well-determined value, which provides the normalization; i.e.,

$$\Delta N(< m_{\rm norm}) = \frac{\left[\int_{m_{\rm min}}^{m_{\rm norm}} \xi(\log m)\, d\log m\right]_{\rm IMF} - \left[\int_{m_{\rm min}}^{m_{\rm norm}} \xi(\log m)\, d\log m\right]_{\rm PDMF}}{\left[\int_{m_{\rm min}}^{m_{\rm norm}} \xi(\log m)\, d\log m\right]_{\rm IMF}} \quad (19)$$

for the number density and equivalently for the mass density. From Figure 5, we get $\Delta N_{\rm sys}(\lesssim 0.4\ M_\odot) \approx 60\%$, $\Delta M_{\rm sys}(\lesssim 0.4\ M_\odot) \approx 35\%$ for M35 at ~175 Myr.

On the other hand, as will be discussed in § 7, small variations between the low-mass parts of the IMFs in various clusters might stem from various levels of turbulence related to the cluster mean density (see, e.g., Myers 1998). If confirmed, the difference in BD detection, for instance between isolated regions such as Taurus ($n \sim$ 1–10 pc^{-3}) and high-density star-forming regions such as, e.g., Orion, Ophiucus, or Trapezium ($n \sim 10^3$–10^4 pc^{-3}), might thus reflect the importance of the level of turbulence in the cloud on the low-mass end of the IMF. As shown in Figure 5, however, for a mean density above $\gtrsim 10^3$ pc^{-3}, these effects do not seem to yield drastically different IMFs, suggesting a universal, dominant process in star formation both in young clusters and in the Galactic field.

2.3. The Planetary Mass Function

Over a hundred planets orbiting stars outside the solar system have now been discovered, with periods $P \lesssim 1500$ days. A statistical analysis of their mass distribution, corrected for the uncertainty due to the inclination $\sin i$ of the orbital plane on the sky, has been established by different authors (Zucker & Mazeh 2001; Jorissen, Mayor, & Udry 2001). The resulting planetary mass distribution dN/dm_p peaks around ~1–2 $M_{\rm Jup}$, due to present detection limits of radial velocity surveys to detect smaller objects, and decreases rapidly to reach essentially zero at ~10 $M_{\rm Jup}$, with only four systems extending up to 16 $M_{\rm Jup}$. This distribution corresponds to a relatively flat MF $\xi(\log m) \approx$ constant below ~10 $M_{\rm Jup}$ (Zucker & Mazeh 2001). This mass distribution differs completely from the stellar+BD mass function derived in § 2.1.4 and clearly points to a different population of substellar objects, namely, *planetary* companions of stars, which formed from a different mechanism than the one yielding the IMF (eq. [17]). It is interesting to note that these planets are now found with a large distribution of eccentricities, from near zero to large eccentricity, suggesting complex mechanisms of dynamical interactions (Udry, Mayor, & Queloz 2003). As mentioned above, the overwhelming majority of these planetary companions have masses near ~1 $M_{\rm Jup}$, significantly below the deuterium-burning minimum mass of $\simeq$12 $M_{\rm Jup}$ (Saumon et al. 1996; Chabrier et al. 2000b), confirming the fact that this mechanism is unlikely to play any specific role in either stellar or planet formation. Notice that this cannot be due to an observational bias since the majority

of these surveys are also intended to detect BD companions of solar-type stars and could easily detect companions up to $\sim$100 $M_{\rm Jup}$.

Zucker & Mazeh (2001) compared the distribution of *stellar companions* of G and K stars with the aforementioned distribution of exoplanets to these solar-type stars. This comparison highlights the lack of objects in the mass range $\sim$10–100 $M_{\rm Jup}$, compared with substantial fraction of companions on both sides of this mass range. This defines the brown dwarf desert, which prompted Zucker & Mazeh to identify two distinct populations of objects originating from two distinct process of formation, namely, the stellar companions and the planetary companions. It would be interesting to extend this argument to other stellar populations, in particular to M dwarfs. Indeed, as mentioned in § 2.1.3, the brown dwarf desert illustrates the lack of companions of solar-type stars in the BD regime, i.e., with large mass ratio $q = m_2/m_1 < 0.1$, compared with *planetary* companions, and does not preclude a substantial fraction of BD companions of smaller mass stars, i.e., of M dwarfs, as suggested by recent determinations (Gizis et al. 2001; Close et al. 2003). Therefore, there should not be any BD desert in the M-dwarf domain. However, if the fraction of planets appears to be the same around M dwarfs as around solar-type stars, their mass distribution should be quantitatively and qualitatively different from the IMF (eq. [17]). While the latter decreases with decreasing mass below about the hydrogen-burning limit (in logarithmic scale) (Fig. 1), the former one should be rising, or flat, below $\sim$10 $M_{\rm Jup}$. It is thus interesting to search for substellar companions around M dwarfs to find out whether the fraction of companions rises or decreases below a certain mass. Since, given our present ignorance of the exact formation history of stars, BDs, or planets, it is impossible to distinguish BDs from planets,[7] a rising distribution of low-mass companions around M dwarfs would be the signature of a population of planets around these stars.

A comparable argument to identify two very distinct populations could stem eventually from the evaluation of their space densities, by comparing the space density of exoplanets with the density of BDs with masses $m < 10$ $M_{\rm Jup}$. From the IMF (eq. [17]), the latter is $\sim$0.025 pc^{-3}. Most of the planets discovered today orbit solar-type stars. About 7% of these stars have a planetary companion of mass $m_p \gtrsim 0.5$ $M_{\rm Jup}$ and orbital period $P \lesssim 4$ yr. This yields a density of planets around solar-type stars $n_P \approx 0.07 \times (1.0 \times 10^{-2}) \approx 10^{-3}$ pc^{-3}. This is obviously a lower limit since (1) only solar-type stars have been surveyed with enough accuracy, (2) only giant planets are accessible to present detections, and (3) only planets with periods shorter than $\sim$1500 days have been detected.[8] If the same fraction of planetary companions applies to M dwarfs, for example, n_P rises by about a factor of 10, and the density of planetary companions becomes comparable with the density of low-mass BDs. Present detections, however, do not allow robust conclusions to distinguish BDs from planets from their estimated space densities.

3. THE SPHEROID MASS FUNCTION

In this paper, we define the spheroid as the Galactic component described by a de Vaucouleurs $\rho(r) \propto e^{-r^{1/4}}$ or a Hubble $\rho(r) \propto 1/r^3$ density profile. It is often called also the stellar halo, in opposition to the isothermal dark halo.

The direct determination of the spheroid LF is a very difficult task, since the population of the thick disk, with a scale height $\sim$1–1.5 kpc, contributes appreciably to star counts up to at least $V \sim 20$, $I \sim 19$. Furthermore, a major difficulty of photometric surveys at large magnitude is distinguishing stars from galaxies. These difficulties are in principle circumvented with *HST*, which can distinguish stars from galaxies to a limit magnitude $I \simeq 23$, avoiding serious contamination from disk stars (Gould, Flynn, & Bahcall 1998, hereafter GFB98), but the small field of *HST* yields statistics too small to derive a robust LF. One thus relies on ground-based observations, where the spheroid population in the solar neighborhood is identified from its kinematic properties. The most recent determination of the subdwarf sample of Luyten's LHS Catalogue was obtained by Dahn et al. (1995), updated recently (C. Dahn & H. C. Harris 2002, private communication). The 298 stars in the sample have a tangential velocity with respect to the local standard of rest $v_{\rm tan} > 220$ km s^{-1}, a strong indication of a stellar halo population, and most of them have a determined parallax. The volume density is determined by the usual $1/V_{\rm max}$ method, where the volume limit is set by both apparent magnitude and proper-motion observational constraints. This yields a $1/\xi = 2.35$ correction factor to account for stars excluded from the sample by selection criteria (C. Dahn 2002, private communication). The faint end of this LF has been confirmed recently by Gizis & Reid (1999) and by the photometric and kinematic identification of halo stars in the fourth Catalogue of Nearby Stars (Fuchs & Jahreiss 1998). Another recent photometric determination is based on a reduced proper-motion analysis of the Revised NLTT Catalog, which contains about 5000 halo stars to a completeness limit $V \sim 18$ (Gould 2003).

These kinematically determined samples must be corrected for incompleteness. As pointed out by Bahcall & Casertano (1986, hereafter BC86), the completeness correction factor de-

[7] The only difference between a giant planet such as Jupiter or Saturn and a BD is the presence of a rock+ice core of several Earth masses at the very center of these planets, reminiscent of the protoplanetary disk from which they were formed. But the only *indirect* clue about the presence of this core stems from the very accurate determinations of the gravitational moments of the planet from *Voyager*, *Pioneer*, and *Galileo*. Such data are obviously unavailable for the exoplanets.

[8] As pointed out by M. Mayor, in the aforementioned mass-period range, our solar system has no giant planet!

pends on the assumed spheroid kinematics. Following GFB98, we adopt the three-component Galactic model of Casertano, Ratnatunga, & Bahcall (1990), which includes a thin disk, a thick disk, and a spheroid component. This model yields an excellent agreement with the spheroid RR Lyrae population (GFB98; Gould & Popowski 1998). With this spheroid kinematic model, GFB98 estimate the completeness factor for spheroid subdwarfs with $v_T > 220$ km s^{-1} to be $\xi = 0.54$. Following the same procedure as these authors, we thus multiply the C. Dahn (2002, private communication) data by a factor $1/(2.35 \times 0.54) = 0.79$. Figure 6 displays the four aforementioned subdwarf LFs, all corrected for incompleteness with factors consistent with the aforementioned Casertano et al. (1990) kinematic model. Significant differences exist between these various determinations. The most recent analyses (C. Dahn 2002, private communication; Gould 2003) predict a significantly larger number of halo subdwarfs for $M_V \gtrsim 8$ than the previous BC86 determination once the $1/\xi = 3.0$ BC86 correction factor has been applied.[9] This points to a larger incompleteness factor than admitted in the BC86 analysis. As noted by Gizis & Reid (1999), the BC86 LF, based on Eggen's (1979, 1980) survey of southern ($\delta < 30$) stars with $\mu > 0\farcs7$ yr^{-1}, might be underestimated by ~30% because of the incompleteness of Eggen's sample in the Galactic plane.

Differences between the *HST* and nearby LFs might be due to *HST*'s small field of view. On the other hand, it is generally admitted that the spheroid is substantially flattened, with $q \sim 0.7$, so that most of the local subdwarfs would reside close to the disk, and this population would not be included in the *HST* sample (see, e.g., Digby et al. 2003). Sommer-Larsen & Zhen (1990) estimate this subdwarf fraction to be about 40%. For this reason, the local normalization of the spheroid subdwarf density from the number density observed at large distances from the plane, as done with *HST* (GFB98), is a very uncertain task. We note also some difference at the ~2 σ level between the C. Dahn (2002, private communication) LF and the NLTT one (Gould 2003), the latter rising more steeply and peaking at a magnitude ~1 mag brighter. The reason for such a difference is unclear. It might stem from the limited statistics in the Dahn et al. survey (~10–30 stars per bin in the $M_V = 9$–12 range) or from the simple color-magnitude relations adopted by Gould (2003). On the other hand, Dahn et al. used a purely kinematic criterion to select halo objects in their sample. As acknowledged by these authors themselves, this undoubtedly rejects bona fide spheroid subdwarfs as a result of their directional locations in the sky. Even such a small correction might be consequential in the last bins. Incompleteness of the LHS Catalogue at faint magnitude would also affect the faint part of the LF. All these uncertainties must be kept in mind when considering the present results.

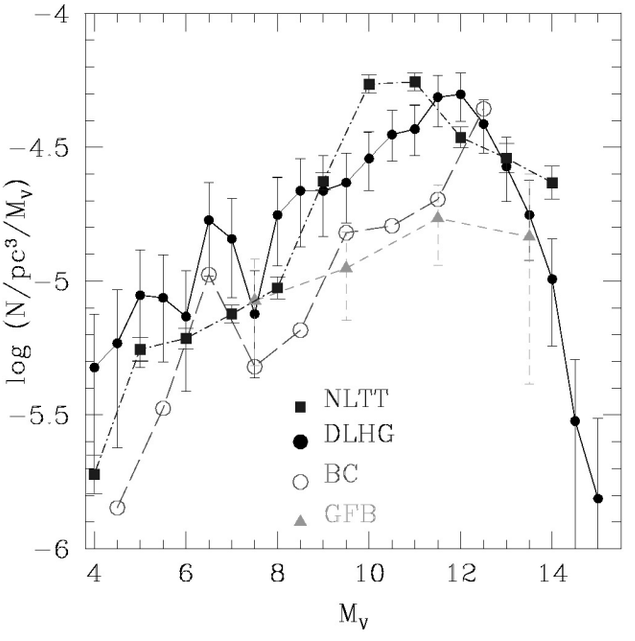

FIG. 6.—*V*-band luminosity function of the Galactic spheroid (stellar halo). *Filled circles and solid line:* Dahn et al. (1995), completed by C. Dahn & H. Harris (2002, private communication); *filled squares and dash-dotted line:* NLTT survey (Gould 2003); *open circles and long-dashed line:* BC86; *shaded triangles and short-dashed line: HST* (GFB98). All LFs have been recalculated with a completion factor based on the Casertano et al. (1990) kinematic model (see text).

The spheroid population can also be identified photometrically, which strongly correlates with metallicity. Figure 7 displays the 114 spheroid stars identified in the Dahn et al. (1995) survey in a M_V-$(V-I)$ color-magnitude diagram as well as the observed thin-disk M-dwarf sequence (Monet et al. 1992; *small dots*) and superposed to the observations five 10 Gyr isochrones with metallicities [M/H] $= -2.0, -1.5, -1.3, -1.0$, and -0.5. Recall that these isochrones reproduce reasonably accurately the observed sequences of various globular clusters of comparable metallicity, except for the more metal rich ones ([M/H] $\gtrsim -1.0$; see BCAH97 and § 1.3). This figure clearly shows that the kinematically identified spheroid subdwarf population covers a wide range of metallicities, from ~1% solar to near solar, with an average value $\langle$[M/H]$\rangle \simeq -1.0$ to -1.3, i.e., [Fe/H] $\simeq -1.7$ to -1.4 (see also Fuchs, Jahreiss, & Wielen 1999).[10] Such a large dispersion remains unexplained and is at odds with a burst of star formation in the spheroid ~10–12 Gyr ago. Accretion during the star orbital motion across the disk is unlikely. A Bondi-Hoyle accretion rate, most likely an upper

[9] Note that the BC86 spheroid LF displayed in Figs. 6 and 7 of Dahn et al. (1995) was *not* corrected by this factor (C. Dahn 2002, private communication).

[10] For metal-depleted objects, a metallicity [M/H] corresponds to an iron-to-hydrogen abundance [Fe/H] $\simeq$ [M/H] $-$ 0.35, due to the α-element enrichment (see BCAH97).

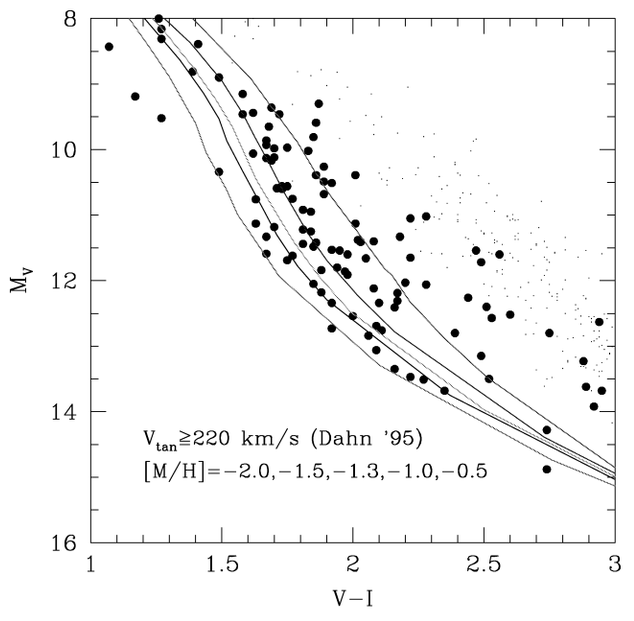

FIG. 7.—Color-magnitude diagram for the Dahn et al. (1995) subdwarf sample with $v_{\rm tan} \geq 220$ km s^{-1}. Superposed are the 10 Gyr isochrones of BCAH97 for [M/H] = −2.0, −1.5, −1.3, −1.0, and −0.5, from left to right. The small dots indicate the Monet et al. (1992) solar-metallicity local sample.

limit except possibly during the early stages of evolution, yields

$$\dot{m}_{\rm acc} \approx 2\pi (Gm)^2 n m_{\rm H}/v^3$$
$$\approx 2.6 \times 10^{-19} \left(\frac{m}{M_\odot}\right)^2 \frac{n}{1\ {\rm cm}^{-3}} \left(\frac{v}{220\ {\rm km\ s}^{-1}}\right)^{-3} M_\odot\ {\rm yr}^{-1},$$

i.e., $m_{\rm acc} \lesssim 10^{-9}\ M_\odot$ for subdwarf masses in 10 Gyr (here n is the density of the ISM and v is the velocity of the star). An alternative possibility is a metallicity and velocity gradient along the spheroid vertical structure above the disk. In that case, the subdwarfs discovered with *HST* should be more metal depleted than the one in the local sample. Recent observations (Gilmore, Wyse, & Norris 2002) have detected a substantial population of stars a few kiloparsecs above the Galactic disk with kinematic properties (rotational velocity and velocity dispersion) intermediate between the canonical thick disk and the spheroid. These authors interpret this "vertical shear" as an extension of the thick disk caused by the ancient merging of a nearby galaxy. This interpretation confirms the previous analysis of Fuchs et al. (1999) and is supported by the recent analysis of Fuhrmann (2002), who finds that the majority of subdwarfs within 25 pc from the Sun with large space velocities $[(U^2 + V^2 + W^2)^{1/2} \gtrsim 100$ km s$^{-1}]$ have a chemical composition characteristic of the thick disk ([Fe/H] $\lesssim -0.5$, [Fe/Mg] ≈ -0.5). If this interpretation is confirmed, this implies a substantial revision of the thick-disk and spheroid models. In that case, the local subdwarf sample and the one observed with *HST* probe two different stellar populations. In particular, as discussed by BC86, the inclusion of a few stars with high velocity belonging to this extended thick-disk population in the local genuine spheroid subdwarf sample will yield a severe overestimate of the supposed spheroid density. Until this issue is solved, we will assume that the NLTT (Gould 2003) or LHS (Dahn et al. 1995; C. Dahn 2002, private communication) samples are representative of the spheroid one,[11] keeping in mind that these samples may include a fraction of thick-disk stars with high dispersion velocities. Such an assumption yields the *maximum* mass contribution and local normalization of the Galactic spheroid component.

A correct analysis of the subdwarf metallicity would require a statistical approach, but the metallicity probability distribution for these stars is presently unknown, and the derivation of such a distribution from a two-color criterion only is of weak significance. For this reason, we have converted the observed LFs of Figure 6 into MFs, based on the BCAH97 mass-M_V relationships, assuming that all stars have a given metallicity. In order to estimate the uncertainty on the MF due to possible metallicity variations, we have used m-M_V relationships for [M/H] = −1.5, −1.0, and −0.5. Figure 8 displays the MF derived from the NLTT LF for these three metallicities. To illustrate the uncertainty due to the different LFs, the MF derived from the C. Dahn (2002, private communication) LF is also shown, for [M/H] = −1.0 (*dotted line*). Interestingly enough, the differences between the MFs derived for the three different metallicities remain modest, a consequence of the limited effect of metallicity in the aforementioned range on the slope dM_V/dm of the MMR (BCAH97). The effect is dominant at the low-mass end of the MF: the lower the metallicity, the steeper the MF. The wiggly behavior of the MF derived from the Dahn et al. LF, with a peak around $\log m = -0.2$ followed by a dip, stems from the flattening behavior of both their LF and the m-M_V relation in the $M_V \approx 8$–10 range.

The MF is reasonably well described by the following log-normal form below 0.7 $M_\odot$, illustrated by the solid line in Figure 8:

$$\xi(\log m) = 3.6 \times 10^{-4} \exp\left\{-\frac{[\log m - \log (0.22 \pm 0.05)]^2}{2 \times 0.33^2}\right\},$$
$$m \lesssim 0.7\ M_\odot. \qquad (20)$$

Although an IMF similar to the disk one (eq. [17]) cannot be totally excluded, in particular if the Dahn et al. (1995) LF happens to be more correct than the Gould (2003) one, equation (20) gives a better representation of the data. For comparison, the IMF derived from the *HST* LF decreases as a straight line

[11] Note that the NLTT LF of Gould (2003) is in agreement with the one derived recently from a detailed reduced proper motion analysis of the Sloan and SuperCosmos surveys (Digby et al. 2003), presumably probing the genuine spheroid subdwarf population.

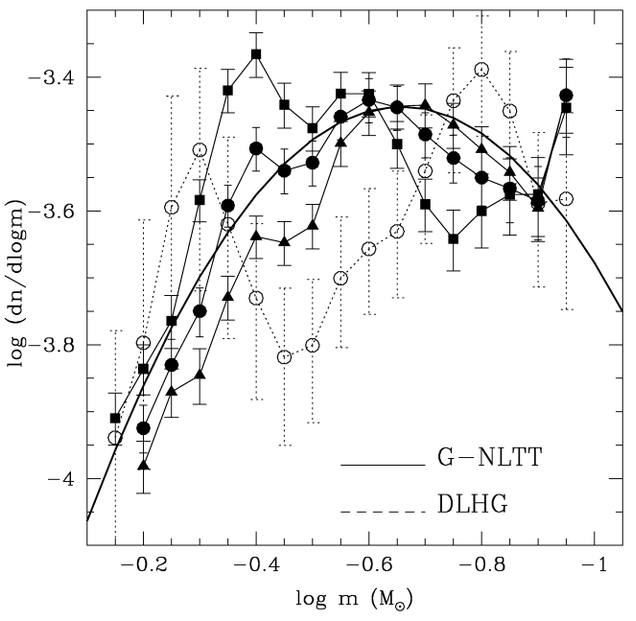

FIG. 8.—Mass function of the Galactic spheroid, based on the NLTT (Gould 2003) LF (*solid lines*) and the BCAH97 mass-M_V relationship, for three metallicities: [M/H] = −1.5 (*filled triangles*), −1.0 (*filled circles*), and −0.5 (*filled squares*). *Dotted line:* same calculation based on the Dahn et al. (1995), C. Dahn (2002, private communication) LF and [M/H] = −1.0 models. *Solid curve:* Parameterization given by eq. (20).

$\xi(\log m) \propto m^{0.25}$ below 0.7 $M_\odot$ (GFB98), a consequence of the much smaller number of faint subdwarfs detected by *HST*, as noted previously (Fig. 6).

For an age $t > 10$ Gyr, a lower limit for the spheroid, stellar evolution either on or off the MS affects objects with mass $m \gtrsim 0.7\ M_\odot$, i.e., $M_V \lesssim 6$. Objects brighter than this magnitude must then be ignored for the IMF determination and normalization. The shape of the IMF above the turnoff mass ($\lesssim 0.9\ M_\odot$ for $t > 10$ Gyr) is undetermined. Various analyses of the high-mass part of the IMF in the LMC, SMC, and various spheroidal galaxies (Massey 1998 and references therein) seem to be consistent with a Salpeter slope, for all these metal-depleted environments. We thus elected to prolongate the IMF (eq. [20]) by such a power law, with a common normalization at 0.7 $M_\odot$, yielding the global spheroid IMF given in Table 2.

Equation (20) yields a normalization at 0.70 $M_\odot$ of $\xi(\log m)_{0.7} = (1.13 \pm 0.5) \times 10^{-4}$ $(\log M_\odot)^{-1}$ pc^{-3}. This yields a spheroid main-sequence star number density $n_{\rm MS} \simeq (2.4 \pm 0.1) \times 10^{-4}$ pc^{-3} and mass density $\rho_{\rm MS} \simeq (6.6 \pm 0.7) \times 10^{-5}\ M_\odot$ pc^{-3}. Note that this value is more than 2 times larger than the determination of GFB98 because of the different IMFs, as mentioned above. Note that we assumed that the power-law form extends to 0.7 $M_\odot$. Given the unknown slope of the IMF for spheroid stars in this mass range, we could have chosen 0.9 $M_\odot$ for the limit of the power-law part of the IMF and extended the lognormal form to this limit. The difference

TABLE 2
IMFs FOR THE VARIOUS COMPONENTS OF THE GALAXY

Parameter	Disk and Young Clusters	Globular Clusters	Spheroid
$m \le m_{\rm norm}$ $[M_\odot]$, $\xi(\log m) = A \exp[-(\log m - \log m_c)^2/2\sigma^2]$			
$m_{\rm norm}$	1.0	0.9	0.7
A	$0.158^{+0.051}_{-0.046}$		$(3.6 \pm 2.1) \times 10^{-4}$
m_c	$0.079^{-0.016}_{+0.021}$	0.33 ± 0.03	0.22 ± 0.05
σ	$0.69^{-0.01}_{+0.05}$	0.34 ± 0.04	0.33 ± 0.03
$m > m_{\rm norm}$ $[M_\odot]$, $\xi(\log m) = Am^{-x}$			
$m_{\rm norm}$	1.0	0.9	0.7
A	4.4×10^{-2}		7.1×10^{-5}
x	1.3 ± 0.3	1.3 ± 0.3	1.3 ± 0.3

in the derived densities, however, is small and largely within the present uncertainties of the IMF. Integration of this IMF in the substellar regime yields a negligible BD number density $n_{\rm BD} \lesssim 3 \times 10^{-5}$ pc^{-3} and mass-density contribution $\rho_{\rm BD_{sph}} \lesssim 2 \times 10^{-6}\ M_\odot$ pc^{-3}.

The mass density of the spheroid must include upper main sequence and evolved stars ($0.7 \lesssim m/M_\odot \lesssim 0.9$) and remnants, with progenitor masses above 0.9 $M_\odot$. Integration of the presently derived IMF yields for these contributions, respectively, $\rho_{\rm ev} \approx 0.8 \times 10^{-5}\ M_\odot$ pc^{-3} and $n_{\rm rem} \approx (2.7 \pm 1.2) \times 10^{-5}$ pc^{-3} (assuming a Scalo coefficient, $x = 1.7$ for $m > 0.7\ M_\odot$, as in GFB98, yields $n_{\rm rem} \approx 1.9 \times 10^{-5}$ pc^{-3}); i.e., for an average WD mass $\langle m_{\rm WD} \rangle = 0.65\ M_\odot$, a remnant WD mass density $\rho_{\rm WD} \approx (1.8 \pm 0.8) \times 10^{-5}\ M_\odot$ pc^{-3}, similar to previous determinations (GFB98). This yields the spheroid total stellar mass density $\rho_{\rm sph} \approx (9.4 \pm 1.0) \times 10^{-5}\ M_\odot$ pc^{-3}, about 1% of the local dark matter density, and a local stellar+BD normalization $\rho_{\rm sph}/\rho_{\rm disk} \approx 1/600$ (see Table 3), in agreement with estimates based on the fourth Catalogue of Nearby Stars (Fuchs & Jahreiss 1998). The corresponding microlensing optical depth toward the LMC is $\tau_{\rm sph} \simeq 10^{-9}$. As discussed earlier, this represents an *upper limit* for the true spheroid mass density, since a fraction of the local subdwarf population identified in Figure 6 might belong to the high-velocity tail of the extended thick-disk population, of which local normalization is about 2 orders of magnitude larger.

The present determinations yield, for an average WD mass upper limit 1.4 $M_\odot$, a *maximum* spheroid WD mass density $\rho_{\rm WD} \lesssim (3.8 \pm 1.7) \times 10^{-5}\ M_\odot$ pc^{-3}, i.e., less than 0.7% of the dark matter local density. As mentioned above, however, the normalization of the spheroid MF is not as straightforward as one would wish since all the BC86, NLTT, *HST*, and parallax surveys are affected by completeness correction factors, determination of which depends on the assumed Galactic model and corresponding asymmetric drift and velocity dispersion for the population identified as the spheroid one. Since the previously derived normalization at 0.7 $M_\odot$ is directly proportional to the $1/\xi$ correction factor in the LF, the detection of a genuine spheroid WD population exceeding 1% of the dark matter density would imply a correction factor larger by a factor of $\gtrsim 2$

near $M_V \sim 6$. A more plausible explanation, as discussed above, is that the thick-disk population extends well above the ~1 kpc scale height and includes a partially pressure supported population. The identified high kinematic WD population would thus be the remnant of the high-mass tail of this relic population dating from the early epoch of the disk formation. An alternative explanation, finally, would be a radically different IMF for $m > 0.9\ M_\odot$ in the halo, an issue addressed in the next section.

Note that the IMF (eq. [20]) is not corrected for binaries. The fraction of subdwarfs in binary systems is presently unknown but it is probably smaller than the one in the disk (Gizis & Reid 2000). Since, as examined in the next section, the spheroid and globular cluster populations seem to originate from a similar IMF, we assume that the binary fraction is similar, i.e., ~15%–20% (Albrow et al. 2001), and thus small enough not to affect significantly the present determination. Note that even if the binary fraction is similar to the disk one, this should not affect the present normalization at $0.7\ M_\odot$ by more than ~10%. However, as illustrated in § 2 for the disk and young cluster populations, a binary fraction in globular clusters and in the spheroid comparable to the disk one (~50%) would bring the spheroid IMF in reasonable agreement with the disk one, an issue of prime importance for assessing the dependence of the IMF upon metallicity.

Although, as mentioned above, the determination of the spheroid IMF and density, and the very identification of the spheroid population itself, relies on much weaker grounds than for the disk, the following conclusions seem to be reasonably robust: (1) the dynamical contribution of the spheroid to the Galactic mass budget is negligible; (2) the IMF is very likely lognormal below $\sim 0.9\ M_\odot$, with a characteristic mass near ~ 0.2–$0.3\ M_\odot$, above the one inferred for the disk IMF, *if* indeed the binary fraction in the spheroid is significantly smaller than the one in the disk; (3) the main contribution to the spheroid mass budget comes largely (~75%) from main-sequence stars (see Table 3), and the spheroid BD population is negligible; and (4) an identified WD population with halo-like kinematic properties exceeding 1% of the dark matter density would imply either a completely different spheroid kinematic model, suggesting that present surveys are severely incomplete in the identification of the spheroid population, or a different original population, implying a thick-disk population with low angular momentum support extending well above the plane, or an IMF peaked in the WD-progenitor mass range.

4. THE GLOBULAR CLUSTER MASS FUNCTION

Globular clusters provide a particularly interesting testbed to investigate the stellar MF. They provide a homogeneous sample of MS stars with the same age, chemical composition, and reddening; their distance is relatively well determined, allowing straightforward determinations of the stellar LF; and the binary fraction is negligible (~10%–20%; Albrow et al. 2001), so the correction due to unresolved binaries on the LF is insignificant. From the theoretical point of view, as mentioned in § 1.3, accurate evolutionary models exist that reproduce the observed color-magnitude diagrams of various clusters with metallicity [M/H] ≤ -1.0 in both optical and infrared colors, down to the bottom of the main sequence (BCAH97; Pulone et al. 1998; King et al. 1998; De Marchi et al. 2000), with the limitations in the optical mentioned in § 1.3 for more metal rich clusters ([M/H] $\gtrsim -1.0$). As discussed in § 1.3, however, the consequences of this shortcoming on the determination of the MF remain modest.

The major problem in determining the IMF of globular clusters is the inclusion of its dynamical history from present-day observations. Dynamical evolution arises from the fact that (1) N-body systems evolve toward energy equipartition and gravitational equilibrium by expelling less massive objects to the cluster periphery, while the most massive ones accumulate toward the center; and (2) interactions with the Galactic potential, interstellar clouds, or other clusters along the orbit lead to evaporation of the cluster with time. Both effects lead to a mass segregation of stars with time and space. The characteristic timescale for mass segregation for a cluster of total mass $M_{\rm tot}$ is about the cluster mean dynamical relaxation time, i.e., its relaxation time near the half-mass radius R_h (in pc) (Meylan 1987):

$$t_{\rm relax} \simeq 9 \times 10^5 \frac{M_{\rm tot}^{1/2}}{\langle m \rangle} \frac{R_h^{3/2}}{\log\,(0.4 M_{\rm tot}/\langle m \rangle)}\ \ {\rm yr}. \qquad (21)$$

This relaxation time is only an approximate dynamical time, since the relaxation timescale strongly varies with mass (as obvious from the dependence on $\langle m \rangle$) and distance from the core, but it gives an estimate for the dynamical timescale of the cluster. It is clear, in particular, that the relaxation time is shortest near the center, where the most massive stars (and thus larger $\langle m \rangle$) accumulate. The relaxation time near the core can be written (Meylan 1987)

$$t_{\rm core} \simeq 1.5 \times 10^7 \frac{1}{\langle m_0 \rangle} \frac{v_c R_c^2}{\log\,(0.5 M_{\rm tot}/\langle m \rangle)}\ \ {\rm yr}, \qquad (22)$$

where R_c is the core radius (in pc), v_c is the velocity scale (in km s^{-1}), and $\langle m_0 \rangle$ is the mean mass of stars in thermal equilibrium in the central parts.

This dynamical issue has been addressed in particular by Paresce & De Marchi (2000). These authors used standard multimass Michie-King models to quantify this effect on the presently observed LF as a function of radial position from the center. They found that mass segregation can affect significantly the regions either inside or beyond the half-light radius r_h, but that near r_h, the deviations from the cluster global MF are insignificant (Fig. 4 of Paresce & De Marchi 2000). Therefore, for clusters whose LF has been measured at significant distance from r_h, mass segregation must be accounted for to determine the global MF from the local one. Otherwise, the global MF will appear steeper than it really is. To estimate the effect of

tidal disruption, Paresce & De Marchi (2000) examined the evolution of the ratio $\Delta \log N$ of lower to higher mass stars in the observed cluster sequences, similar to equation (19). Indeed, this parameter is likely to be the most relevant one to describe the region affected by external and internal dynamics. The value of $\Delta \log N$ for 12 clusters was found to exhibit no specific trend in particular with the cluster disruption time, an indication of tidal disruption effects. In other words, Paresce & De Marchi found no obvious dependence of the 12 deep LFs on the cluster dynamical history, in spite of the very different cluster conditions, with the noticeable exception of NGC 6712 (De Marchi et al. 1999), which is probably close to complete disruption. These results are consistent with the fact that the 12 clusters examined by Paresce & De Marchi (2000) are located well inside the survival boundaries of the vital diagrams obtained from numerical simulations (Gnedin & Ostriker 1997). This suggests that the clusters probably remained undisturbed in their internal regions. Therefore, the MF measured near the half-light radius for these clusters should resemble very closely the IMF.

The most striking conclusions of the study of Paresce & De Marchi (2000) are that (1) a single power-law MF cannot reproduce both the bright part and the faint part of the observed LFs and (2) the PDMFs derived for all the clusters are consistent with the same lognormal form peaked at $m_c = 0.33 \pm 0.03\ M_\odot$, with a standard deviation $\sigma = 0.34 \pm 0.04$, the error bars illustrating the variations between all clusters:

$$\xi(\log m) \propto \exp\left\{-\frac{[\log m - \log (0.33 \pm 0.3)]^2}{2(0.34 \pm 0.04)^2}\right\}, \quad (23)$$

$$m \leq 0.9\ M_\odot.$$

The limit ~0.8–0.9 $M_\odot$ corresponds to the turnoff mass for an age $t \approx 10$ Gyr for metal-depleted environments.

This MF is displayed by the dashed line in Figure 9, superposed to the MFs derived in the present paper with the BCAH97 MMRs of appropriate metallicity from the 12 cluster LFs observed in both optical (WFPC) and infrared (NICMOS) colors with *HST* by Paresce & De Marchi (2000). These observations are in excellent agreement with observations of the same clusters by other groups. As cautiously stressed by Paresce & De Marchi (2000), however, only four cluster sequences extend significantly beyond the peak of the LF, which corresponds to a mass $m \approx 0.3\ M_\odot$. Future large, deep-field surveys, for example with the *HST* Advanced Camera for Survey (ACS), are necessary to make sure that all the cluster IMFs are adequately reproduced by the aforementioned IMF. Since the latter, however, adequately reproduces the bright part of the LF, i.e., the upper part of the IMF, there seems to be no reason why significant departures would occur at the lower part, except if—contrary to what seems to have been established from either Michie-King models or Fokker-Planck calculations—mass segregation or tidal shocks affect significantly the shape of the

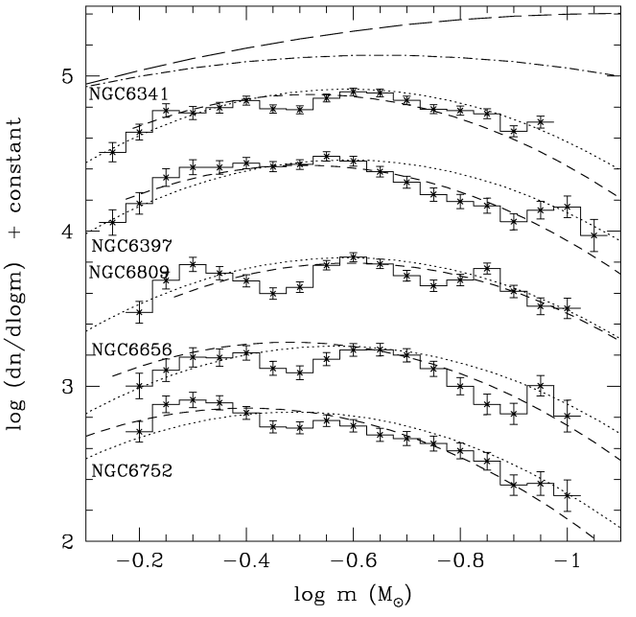

FIG. 9.—Mass function calculated for various globular clusters with the BCAH97 MMRs in several bandpasses, from the LFs of Paresce & De Marchi (2000), spanning a metallicity range $-2.0 \lesssim$ [M/H] $\lesssim -1.0$. The short-dashed and dotted lines display the IMFs (eq. [23]) and (eq. [20]), respectively, whereas the long-dashed and dot-dashed lines at the top illustrate the disk single IMF (eq. [17]) and system IMF (eq. [18]), respectively.

IMF even near the half-light radius, yielding a deficiency of low-mass stars (see, e.g., Baumgardt & Makino 2003), or similarly, if the half-*mass* radius does not correspond to the observed half-*light* radius. The dotted lines in Figure 9 illustrate the IMF derived in the previous section for the spheroid population (eq. [20]), with the characteristic mass shifted by 1–2 σ (i.e., $m_c = 0.22$–$0.32\ M_\odot$). The agreement between the globular cluster and the spheroid IMF is striking, exhibiting similar standard deviations σ and characteristic masses within 2 σ. The slightly larger characteristic mass for globular cluster stems most likely from some dynamical evolution, yielding some evaporation of the objects with mass $\lesssim 0.3\ M_\odot$, even near the half-mass radius. This similarity between the globular cluster and the spheroid MF corroborates the traditional view that globular star clusters and spheroid stars originate from the same stellar population (Fall & Rees 1985). The low mass-to-light ratio of globular clusters compared to comparatively old systems such as elliptical galaxies or bulges of spiral galaxies stems from the dynamical evolution of the clusters, depriving them of their low-mass stellar content. As mentioned earlier, the observed binary fraction in globular clusters is too small (<20%; Albrow et al. 2001) to affect significantly the IMF. Note that this fraction has been determined in the core and thus should represent an *upper* limit for the cluster initial binary fraction. Therefore, the globular cluster IMF (eq. [23]) and spheroid IMF (eq. [20]) are genuinely different from the disk

field IMF (eq. [17]), illustrated by the long-dashed line at the top of Figure 9, providing, as mentioned above, (1) that the cluster MF near the half-mass radius has not been affected significantly by dynamical evolution and (2) that the binary fraction is small. If true, this difference suggests that the IMF characteristic mass is larger for metal-depleted environments, an issue examined in the next section.

5. THE DARK HALO AND EARLY STAR MASS FUNCTION

5.1. The Dark Halo Mass Function

Various constraints exist on the IMF of the Galactic isothermal dark halo [$\rho(r) \propto 1/r^2$], and thus on its baryonic mass content.

1. Star-count observations of the HDF exclude the presence of a significant dark halo main-sequence stellar population (Bahcall et al. 1994; Méra, Chabrier, & Schaeffer 1996; Elson, Santiago, & Gilmore 1996; Graff & Freese 1996; Chabrier & Méra 1997). This implies that the IMF cannot extend below $m \simeq 0.8\ M_\odot$ for a halo age $\tau_H \sim 13$ Gyr.

2. *One* red giant, HE 0107−5140, has been detected recently with the Hamburg/ESO survey (HES), with an iron abundance [Fe/H] $= -5.3 \pm 0.2$ (Christlieb et al. 2002). Note that [Fe/H] is a very good tracer of the composition/metallicity of the surrounding environment, in contrast to C, N, or O, which can be self-processed by the star through the CNO cycle. The inferred mass and effective temperature are $m \approx 0.8\ M_\odot$ and $T_{\rm eff} = 5100 \pm 150$ K, respectively. Given the magnitude limit of the survey ($B_{\rm lim} \sim 17.5$), its detection could be possible at a distance of about 11 kpc, near the edge of the spheroid. Previous surveys were limited to brighter magnitudes within the inner part of the Galactic halo, so the lack of detection of very metal depleted ([M/H] $\ll -4$) stars in the halo population might be an artifact due to too-faint detection limits. The faintest giants in the HES survey extend up to 20 kpc or more. Further analysis of the survey should tell us whether it reveals the tip of the red giant branch of a Population III stellar population.

3. The existence of a significant remnant population in the dark halo is not a completely settled issue yet. As mentioned in the previous section, the maximum contribution from spheroid and/or dark halo WDs predicted by the IMF (eq. [20]) represents at most ∼0.5% of the dark matter density, i.e., $\rho_{\rm WD} \approx 4 \times 10^{-5}\ M_\odot\ {\rm pc}^{-3}$, so the unambiguous detection of a genuine halo WD population with a significantly larger density would imply that the halo IMF differs significantly from this form and peaks in the 1–10 $M_\odot$ mass range. Microlensing observations of dark matter baryonic candidates in the halo, however, remain controversial. The MACHO observations (Alcock et al. 2000) yield a microlensing optical depth based on 13–17 events of $\tau = 1.2^{+0.4}_{-0.3} \times 10^{-7}$, with a total mass in the objects within 50 kpc $M_{50} = 9^{+4}_{-3} \times 10^{10}\ M_\odot$, i.e., ≲20% of the dynamical mass. For a standard isothermal halo model with a velocity dispersion $v_{\rm tan} = 220$ km s^{-1}, the event time distribution corresponds to a peak in the range ∼$0.5 \pm 0.4\ M_\odot$. Since M-dwarf stars are excluded as a significant dark halo population (point 1 above), this implies halo WDs. The EROS project, exploring a larger field around the disks of the LMC and SMC, derived an upper limit contribution to the dark matter of 25% for objects in the mass range $2 \times 10^{-7} \leq m/M_\odot \leq 1$ at the 95% confidence level (Afonso et al. 2003). Interestingly enough, the only events detected today toward the SMC have been shown to belong to the SMC population. One thus cannot exclude that events detected toward the LMC are mainly due to self-lensing events, as pointed out originally by Sahu (1994), or that some events such as supernovae or very long period variables have been misidentified as microlensing events.

Another important constraint on the dark halo population stems from the abundances of helium and heavy elements, which point to a primordial WD mass fraction in the halo $\rho_{\rm WD} \lesssim 0.1\rho_{\rm dyn} \lesssim 10^{-4}\ M_\odot\ {\rm pc}^{-3}$ (Gibson & Mould 1997; Fields, Freese, & Graff 2000). This is confirmed by recent nucleosynthesis calculations of zero or near-zero metallicity low-mass and intermediate-mass stars, which show that helium burning and the CNO cycle process material (in particular C and O) to the surface (Fujimoto, Ikeda, & Iben 2000; Siess, Livio, & Lattanzio 2002).

Several detections of faint, cool, high-velocity WDs in the solar neighborhood, based on either spectroscopic, kinematic, or photometric identifications, have been claimed recently (Oppenheimer et al. 2001). These detections, however, remain controversial and are based on a limited number of objects. Indeed, if the extended thick disk suggested by Gilmore et al. (2002) and Fuhrmann (2002) is confirmed, with kinematic properties intermediate between the standard thick disk and the spheroid ones, a substantial fraction of the high proper motion WDs discovered by Oppenheimer et al. (2001) might indeed belong to this population. As shown by Chabrier (1999), one needs large-field (>1 deg^2) surveys at faint magnitude (V, R, $I > 20$) to really nail down this issue and derive a reasonably robust estimate of the halo WD density.

It thus seems clear that the present dark halo contains only a negligible fraction of the Galactic baryonic mass.

5.2. The Early Star Mass Function

This brings us to the hypothetical determination of the IMF of primordial stars formed at large redshift. Only indirect information on such early star formation processes can be inferred from various observational constraints and from galactic evolution (see, e.g., Larson 1998).

1. The modest increase of metallicity along Galactic history, from [M/H] ≈ −2, characteristic of the spheroid, to [M/H] = 0, but the scarcity of very metal depleted [M/H] $\ll -4.0$ stars in the

Milky Way as well as in other galaxies, the so-called G-dwarf problem, or conversely the similarity of the ratio of massive (oxygen producing) stars to low-mass stars between spheroid and disk, imply that relatively few LMSs were formed when the metallicity was very low at early times.

2. Observations of young galaxies at $z > 1$ in the submillimeter and far-IR domains rule out a Salpeter IMF extending down to the H-burning minimum mass and suggest a top-heavy IMF, with a cutoff near $\sim 0.7\ M_\odot$, to produce massive stars without producing low-mass stars whose light would remain visible to the present time (Dwek et al. 1998; Blain et al. 1999).

3. The observed abundances of heavy elements in clusters of galaxies require an increase by a factor of ~ 3 in the total mass of heavy elements over that predicted by a Salpeter IMF, thus a comparable increase in the ratio of heavy elements per solar mass produced by high-mass stars relative to the number of low-mass stars formed.

4. A top-heavy IMF at early times of galactic evolution increases the number of SNe II per visible stars, providing more excess thermal energy and thus a larger amount of hot gas and heavy elements ejected in the IGM from the bound clusters of galaxies. This is consistent with the fact that most of the heavy elements in clusters are in the IGM rather than in galaxies.

5. Increasing *M/L* ratio and Mg/H and Mg/Fe abundances with mass are observed in early-type galaxies (Worthey, Faber, & González 1992). This points to a larger relative contribution from massive stars, i.e., a dominant high-mass mode formation, and more mass locked in remnants.

6. Recent observations of the large-scale polarization of the cosmic microwave background measured by the *WMAP* satellite require a mean optical depth to Thomson scattering $\tau_e \sim 0.17$, suggesting that reionization of the universe must have begun at large redshift ($z \gtrsim 10$). A possible (but not unique) solution is a top-heavy IMF for primordial, nearly metal free stars (Ciardi, Ferrara, & White 2003; Cen 2003).

Although certainly not conclusive, all these independent constraints (to be considered with caution) point to an early-type IMF with a minimum low-mass cutoff $\gtrsim 1\ M_\odot$. On the other hand, [α-element/Fe] ratios measured in the intergalactic hot gas seem to be only slightly oversolar, which implies a significant contribution from Type Ia SNe, suggesting a constant Salpeter-like slope of the high-mass tail ($m \gtrsim 1\ M_\odot$) of the IMF. Indeed, an IMF with a Scalo slope [$\xi(\log m) \propto m^{-1.7}$] seems to underestimate the fraction of very massive stars to solar-type stars in high-z field galaxies, producing too much long-wavelength light by the present epoch (Lilly et al. 1996; Madau, Pozzetti, & Dickinson 1998).[12]

Indeed, the thermal Jeans mass strongly depends on the temperature ($\propto T^{3/2}$) and more weakly on the pressure ($\propto P^{-1/2}$). Although there is no reason for the latter to have changed significantly during the universe evolution, the temperature did evolve significantly. As pointed out by Larson (1998), the very minimum ambient temperature of the medium is given by the cosmic background radiation $2.73(1 + z)$ K, so the thermal Jeans mass, i.e., the minimum mass for gravitationally bound objects, increases with redshift. Whether this mass is the very characteristic mass in star formation or whether a *distribution* of Jeans masses is more relevant will be examined in § 7. It is also important to note that, in the absence of a significant fraction of metals, the cooling, and thus fragmentation, of the cloud proceeds via collisional excitation and radiative de-excitation of H_2, which cannot cool below 85 K (first rotational level of H_2) (see, e.g., Abel, Bryan, & Norman 2000; Nakamura & Umemura 2002; Bromm, Coppi, & Larson 2002).

Given all this general context, it is interesting to examine the signature of a primordial IMF biased toward large masses ($>1\ M_\odot$) and more specifically toward WD progenitors, i.e., with a characteristic mass in the AGB-mass range, such as the following form:

$$\xi(\log m) = Am^{-1.9} \exp\left[-\left(\frac{3.2\ M_\odot}{m}\right)^{1.6}\right], \tag{24}$$

which is adequately represented also by a form similar to the one used previously for the disk and the spheroid, namely:

$$\xi(\log m) \propto \exp\left\{-\frac{[\log m - \log (3.5)]^2}{2 \times 0.2^2}\right\},\ m \leq 4.0\ M_\odot,$$
$$\xi(\log m) \propto m^{-1.7},\ m \geq 4.0\ M_\odot. \tag{25}$$

This IMF is similar to the one suggested by Chabrier, Segretain, & Méra (1996) and Adams & Laughlin (1996), with a cutoff below $\sim 1\ M_\odot$, but it extends now with a power-law tail $\xi(\log m)_{m \gg 1} \propto \sim m^{-1.7}$ to produce a larger number of SN II progenitors, as discussed above. As shown in the next section, such a remnant-dominated IMF increases the mass-to-light ratio and the relative contribution of WD progenitors to the total mass. Madau & Pozzetti (2000) have examined the constraint on the extragalactic background light $I_{\rm EBL}$ received today on Earth, produced by a burst at time t_F of primordial stars formed with such an IMF. They found out that, for a cosmological model (h; Ω_m; Ω_Λ) = (0.65; 0.30; 0.70), a mass fraction of primordial stars produced by the IMF of Chabrier et al. (1996) as high as $\Omega_* h^2 \simeq 0.30(\Omega_B h^2)$, where $\Omega_B h^2 = 0.0193$ is the BBN baryon density, $\Omega_* = \rho_*/\rho_c$, and $\rho_C = 3H_0^2/8\pi G$ is the universe critical density, is compatible with the observed upper limit for diffuse background light today $I_{\rm EBL_{obs}} \simeq 100$ nW m^{-2} sr^{-1} (Hauser & Dwek 2001), provided that these stars formed at a redshift $z \gtrsim 5$. This is obviously an upper limit since the contributions from subsequent star formation episodes must be added, and these calculations must be considered as purely indicative. Whether the inferred chem-

[12] Note, however, that these results depend on the correction due to dust extinction and should be considered with due caution.

ical enrichment and light production at high redshift are compatible with observations remains to be determined accurately. However, they illustrate the fact that a substantial fraction of baryons could be trapped in a primordial generation of intermediate-mass stars whose remnants would be present today in galactic halos or in the intergalactic medium, provided that they formed at high enough redshift. As noted by Madau & Pozzetti (2000), the returned fraction of gas in that case is about 80% so that the corresponding WD mass fraction today would be less than 10%, consistent with the values discussed in § 5.1.

6. GALACTIC MASS BUDGET, MASS-TO-LIGHT RATIOS

The IMF has different implications in the general process of galaxy formation and evolution, depending on the considered mass range. The chemical enrichment of the galaxies and of the intergalactic medium (IGM), i.e., their heavy-element content and the energy feedback produced by SNe II, depends primarily on stars with $m \gtrsim 10\ M_\odot$, whereas their luminosity results mostly from the stars from about 1 to a few $M_\odot$, and most of the mass is contained in objects with $m \leq 1\ M_\odot$. The relative mass fractions of these different quantities thus bear important consequences for the evolution of the galaxies and their observational signatures (colors, magnitudes). Galactic evolution models generally assume that the IMF is universal and thus does not evolve with time. Given the arguments presented in the previous sections, however, the low-mass cutoff of the IMF may have evolved from the conditions of early star formation, at high redshift, to the ones prevailing in today's spiral galaxy disks, affecting the evolution of mass-to-light ratios (M/L) from early-type galaxies to present-day disk galaxies. Figure 10 displays the evolution of the M/L ratio in optical and infrared bandpasses (from G. Bruzual & S. Charlot 2003, in preparation)[13] obtained with the disk, spheroid, and early-star top-heavy IMFs derived in the previous sections, from 1 to 13 Gyr (i.e., redshift $z \sim 6$ to $z = 0$). The results obtained with a Salpeter IMF over the entire mass range 0.1–100 $M_\odot$ are shown for comparison (*dotted line*). For $t \geq 10$ Gyr, the disk (eq. [17]) and spheroid (eq. [20]) IMFs yield M/L ratios a factor of 1.8 and 1.4 smaller, respectively, than the ones obtained with a Salpeter IMF. This result is in excellent agreement with the values determined in disk galaxies and required for the latter to reproduce the observed Tully-Fischer relation (Sommer-Larsen & Dolgov 2001; Portinari, Sommer-Larsen, & Tantalo 2003). As noted by Portinari et al. (2003), a Salpeter slope for the high-mass tail of the IMF predicts too high gas-to-luminosity fractions and metal yields in spiral disks. Observations tend to favor a high-mass slope somewhere between the Salpeter ($x = 1.35$) and the Scalo ($x = 1.7$) value. This is within the previously mentioned uncertainty of the high-mass part of the IMF (see Table 1), not to mention remaining uncertainties in stellar yield determinations.

Tables 3 and 4 display the relative number and mass fractions over the entire BD+stellar regime obtained with the IMFs derived in the present review, for various mass ranges representing BDs ($m < 0.072\ M_\odot$), low-mass stars (LMSs; $0.072 < m/M_\odot \leq 1$), intermediate-mass stars (IMSs; $1 < m/M_\odot \leq 9$) and high-mass stars (HMSs; $9 < m/M_\odot$), respectively. These fractions are defined as

$$\mathcal{N} = \frac{\int_{\log(m_{\rm min})}^{\log(m_{\rm max})} \xi(\log m)\, d\log m}{\int_{0.001}^{100} \xi(\log m)\, d\log m}, \tag{26}$$

$$\mathcal{M} = \frac{\int_{\log(m_{\rm min})}^{\log(m_{\rm max})} m\xi(\log m)\, d\log m}{\int_{0.001}^{100} m\xi(\log m)\, d\log m}. \tag{27}$$

Tables 3 and 4 give also the inferred present and initial Galactic number and mass densities. As in Chabrier (2001), we take for the disk a white dwarf density $n_{\rm WD} \simeq (5.5 \pm 0.8) \times 10^{-3}$ pc^{-3} (Holberg, Oswalt, & Sion 2002) with an average mass $\langle m_{\rm WD} \rangle = 0.65\ M_\odot$, i.e., a white dwarf mass density $\rho_{\rm WD} \simeq (3.7 \pm 0.5) \times 10^{-3}\ M_\odot$ pc^{-3}, a neutron star density $n_{\rm NS} \simeq 10^{-3}$ pc^{-3} (Popov et al. 2000) with a mass $\langle m_{\rm NS} \rangle = 1.4\ M_\odot$, and a red giant contribution $n_{\rm RG} \simeq 0.3 \times 10^{-3}$ pc^{-3}, $\rho_{\rm RG} \simeq 0.6 \times 10^{-3}\ M_\odot$ pc^{-3} (Haywood, Robin, & Crézé 1997). Recent determinations suggest a *thick-disk* local normalization of ~15%–20%, significantly larger than previous determinations (Soubiran, Bienaymé, & Siebert 2003; Fuhrmann 2002).

7. THE INITIAL MASS FUNCTION THEORY

Several clues to understanding star formation can be deduced from the IMFs determined in the previous sections and from observations of star-forming regions:

1. Star formation in the Galactic disk and in young clusters extends well below the hydrogen-burning limit ($=0.072\ M_\odot$) and very likely below the deuterium-burning limit ($\simeq 0.012\ M_\odot$), with a number density of brown dwarfs comparable to the stellar one.

2. The shape of the IMF seems to be similar in very diverse environments, pointing to a power-law form for large masses and a lognormal distribution at low masses below ~1 $M_\odot$. Within the present (admittedly large) uncertainties concerning the spheroid and primordial star IMF determinations, there is a hint for a characteristic mass decreasing with time, from a few solar masses or more for early star formation conditions at large redshift to ~0.2–0.3 $M_\odot$ for the spheroid and metal-

[13] These values correspond to a birthrate parameter $b = 0$, where $b = \mathrm{SFR}/\langle \mathrm{SFR} \rangle$ is defined as the ratio between the present and past average star formation rate. This corresponds to a burst of star formation at a time $t = 0$ and is thus appropriate for elliptical galaxies. Spiral galaxies are characterized by values of $b \neq 0$ ($b \gtrsim 0.8$ for late spirals) (Kennicutt, Tamblyn, & Congdon 1994), which corresponds to an exponentially decreasing SFR $\propto e^{-t/\tau}$, yielding M/L ratios decreasing with increasing b from the $b = 0$ value.

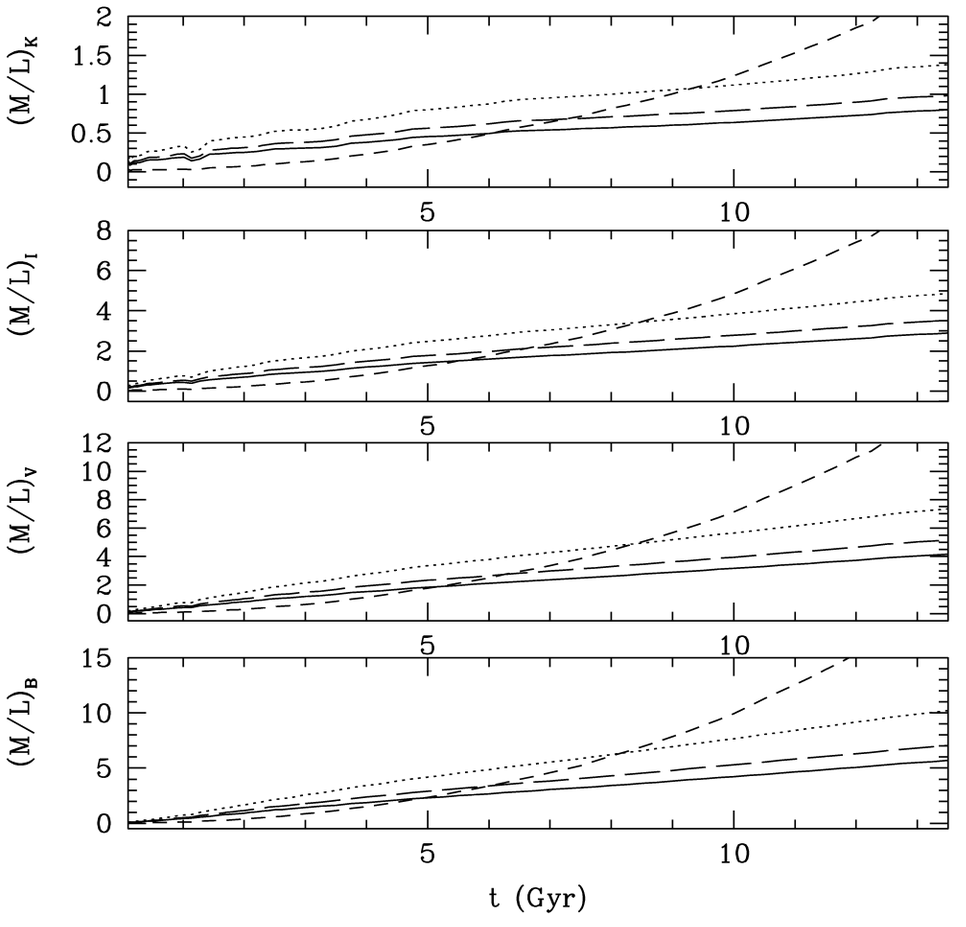

FIG. 10.—Mass-to-light ratios in various passbands, in units of stellar mass per solar luminosity in the considered band, calculated with the Salpeter IMF (*dotted line*), the disk IMF (eq. [17]) (*solid line*), the spheroid IMF (eq. [20]) (*long-dashed line*), and the top-heavy IMF (eq. [24]) (*short-dashed line*). The calculations correspond to simple stellar populations (SSPs), i.e., a stellar birthrate parameter $b = 0$ (see text). All IMFs are normalized to $\int_{0.01}^{100} m(dN/dm)dm = 1$. Courtesy of S. Charlot.

depleted globular clusters and ~0.1 $M_\odot$ for the disk field and young clusters. This assumes a small ($\lesssim$20%) fraction of binaries for the spheroid and the globular clusters. If not, the disk IMF is very likely representative of the spheroid conditions as well. If real, this trend might reflect the effect of the increasing ambient temperature, $T_{\min} = 2.73(1 + z)$ K, with increasing redshift formation, or simply the decreasing ability of the cloud to cool and fragment to smaller scales with decreasing metal abundances. The high-mass parts of these IMFs, however, seem to be very similar, consistent with a Salpeter power law, within $\sim \pm 0.3$ remaining uncertainty in the power-law exponent, for clusters with a factor of ~200 range in densities and a factor of ~10 range in metallicities (Massey 1998; Wyse et al. 2002). The near-uniformity of the IMF seems to extend far beyond the Galaxy. Indeed, a measure of the low mass to high mass ratio is the [Fe/O] ratio, or the α-element ratio. This ratio has been found to be very similar in elliptical galaxies, the intracluster medium (Wyse 1997), and QSO Lyα absorption systems (Lu et al. 1996) and is consistent with a Salpeter IMF at high masses and a flatter IMF at low masses. The same conclusion holds for dwarf-spheroidal galaxies, believed to be dominated by dark matter, finding LFs (and MFs) similar to globular clusters of comparable metallicities for $m \gtrsim 0.3\ M_\odot$ (Wyse et al. 2002). This near-uniformity of the IMF points toward a *dominant self-similar, scale-free process at large scales*, yielding a power-law distribution.

3. Star formation is a rapid process, probably more rapid than the thermal crossing timescale $\tau_S = L/c_s \gtrsim 10$ pc/0.2 km s$^{-1} \approx$ 50 Myr for a cloud of size L and temperature $T \sim 10$ K or the ambipolar diffusion timescale $\tau_{\rm ad} \gtrsim 10$ Myr for a cloud of average density ~10^2 cm^{-3} and $B \approx$ a few μG (Ciolek & Mouschovias 1995), and comparable to the dynamical timescale

TABLE 3
PRESENT-DAY STELLAR AND BROWN DWARF GALACTIC BUDGET

Parameter	Disk	Spheroid	Dark Halo
n_{BD}	0.13 ± 0.06	$\lesssim 3.5 \times 10^{-5}$	
ρ_{BD}	$(0.4 \pm 0.2) \times 10^{-2}$	$\lesssim 2.3 \times 10^{-6}$	
n_* ($\leq 1\ M_\odot$)	0.13 ± 0.02	$\leq (2.4 \pm 0.1) \times 10^{-4}$	
ρ_* ($\leq 1\ M_\odot$)	$(3.5 \pm 0.3) \times 10^{-2}$	$\leq (6.6 \pm 0.7) \times 10^{-5}$	$\ll 10^{-5}$
n_* ($>1\ M_\odot$)	0.4×10^{-2}	0	
ρ_* ($>1\ M_\odot$)	0.6×10^{-2}	0	
n_{rem} (pc^{-3})	$(0.7 \pm 0.1) \times 10^{-2}$	$\leq (2.7 \pm 1.2) \times 10^{-5}$	?
ρ_{rem}	$(0.6 \pm 0.1) \times 10^{-2}$	$\leq (1.8 \pm 0.8) \times 10^{-5}$	
n_{tot}	0.27 ± 0.06	$\leq 3.0 \times 10^{-4}$	
ρ_{tot}	$(5.1 \pm 0.3) \times 10^{-2}$	$\leq (9.4 \pm 1.0) \times 10^{-5}$	$\ll 10^{-5}$
$\mathcal{N}$(BD); $\mathcal{M}$(BD)	0.48; 0.08	0.10; 0.03	
$\mathcal{N}$(LMS); $\mathcal{M}$(LMS)	0.48; 0.68	0.80; 0.77	
$\mathcal{N}$(IMS); $\mathcal{M}$(IMS)	0.015; 0.11	0.0; 0.0	
$\mathcal{N}$(HMS); $\mathcal{M}$(HMS)	0; 0	0.0; 0.0	
$\mathcal{N}$(rem); $\mathcal{M}$(rem)	0.025; 0.13	0.10; 0.20	?

NOTE.—Number densities n are in pc^{-3}; mass densities ρ are in $M_\odot$ pc^{-3}.

$\tau_{dyn} = (3\pi/32G\rho)^{1/2} \approx 10^6 (n/10^3\ \mathrm{cm}^{-3})^{-1/2}\ \mathrm{yr} \approx (1\text{–}5) \times 10^5$ yr for typical star-forming molecular clouds (see, e.g., Elmegreen 2000; Hartmann 2001, 2003; Onishi et al. 2002). This is illustrated in Figure 11, where observations of low-mass objects in young ($\lesssim$1 Myr) clusters are superposed on various theoretical isochrones from Baraffe et al. (2002). Most of the objects tend to pile up above the ~1–3 Myr isochrones. Similar conclusions have been reached for other clusters (see, e.g., Luhman 2000; Najita et al. 2000; Briceño et al. 2002; Hartmann 2003). The position of the few objects located on the left side of the diagram, which appear to be hotter and fainter than the bulk of the data, are interpreted as an effect of strong accretion (Comerón et al. 2003). As shown by Hartmann et al. (1997), the typical accretion rate in young clusters, $\dot{m}_{acc} \approx 10^{-8}$ to 10^{-9} $M_\odot$ yr^{-1} (Hartmann et al. 1998), is too small to affect appreciably the mass of the object, but it can modify its evolution and thus the mass-age relationship. Indeed, the object contracts abruptly to adjust to the accreted material, reducing its radiating surface and mimicking the luminosity of an older nonaccreting object. The stronger the accretion, the larger the effect.

Even though the theoretical isochrones at young ages should be taken with great caution (see § 2.2), it is clear from Figure 11 that the peaked age distribution is different from the one expected from a constant formation rate, for which the number of stars per age interval increases rapidly with time, as would result from star formation history linked to ambipolar diffusion and crossing times (Kenyon & Hartmann 1990). Moreover, the

TABLE 4
INITIAL STELLAR AND BROWN DWARF GALACTIC BUDGET (FROM TABLE 2)

Parameter	Disk	Spheroid
n_{BD}	0.13 ± 0.06	$\sim 3.5 \times 10^{-5}$
ρ_{BD}	$(0.4 \pm 0.2) \times 10^{-2}$	$\sim 2.3 \times 10^{-6}$
n_* ($\leq 1\ M_\odot$)	0.13 ± 0.02	$\leq (2.4 \pm 0.1) \times 10^{-4}$
ρ_* ($\leq 1\ M_\odot$)	$(3.5 \pm 0.3) \times 10^{-2}$	$\leq (6.6 \pm 0.7) \times 10^{-5}$
n_* ($>1\ M_\odot$)	1.5×10^{-2}	$\leq 2.3 \times 10^{-5}$
ρ_* ($>1\ M_\odot$)	4.7×10^{-2}	$\leq 1.0 \times 10^{-4}$
n_{tot}	0.27	$\leq 3.0 \times 10^{-4}$
ρ_{tot}	$(8.6 \pm 0.3) \times 10^{-2}$	$\leq 2.0 \times 10^{-4}$
$\mathcal{N}$(BD); $\mathcal{M}$(BD)	0.48; 0.04	0.10; 0
$\mathcal{N}$(LMS); $\mathcal{M}$(LMS)	0.48; 0.41	0.80; 0.48
$\mathcal{N}$(IMS); $\mathcal{M}$(IMS)	0.04; 0.35	0.09; 0.34
$\mathcal{N}$(HMS); $\mathcal{M}$(HMS)	0; 0.20	0; 0.18

NOTE.—Number densities n are in pc^{-3}; mass densities ρ are in $M_\odot$ pc^{-3}.

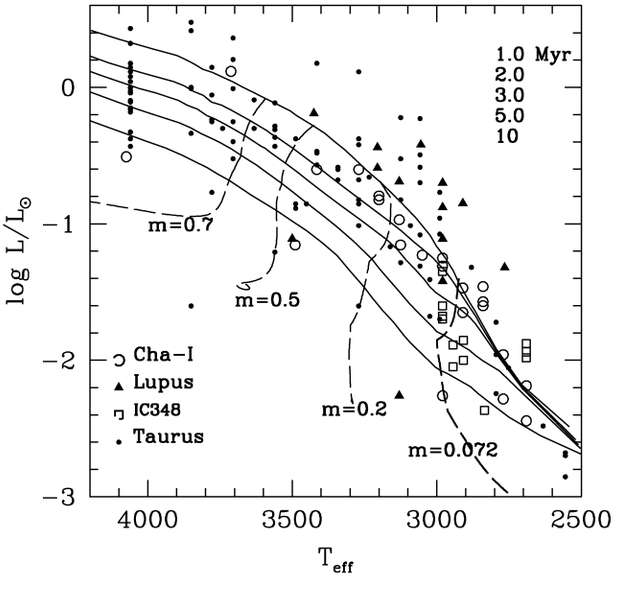

FIG. 11.—Hertzsprung-Russell diagram for young objects in Chameleon (*open circles*), Lupus (*filled triangles*), IC 348 (*open squares*) from Comerón et al. (2003), and Taurus (*dots*) from Briceño et al. (2002). Superposed are various isochrones of Baraffe et al. (2002), for $\tau = 10^6$, 2×10^6, 3×10^6, 5×10^6, and 10^7 yr from top to bottom for different masses, as indicated.

wide dispersal of the *ROSAT* All Sky Survey (RASS) sources is essentially impossible to explain with a 10 Myr old population, given the low velocity dispersions ($\lesssim$10 km s^{-1}) in star-forming regions (Feigelson 1996). More generally, observations of star-forming regions suggest not only that star formation is a rapid process, but that cloud dispersal is fast as well ($\lesssim$10 Myr; Feigelson 1996; Hartmann 2001). This property of star formation points toward a *process dominated by turbulent motions* and the rapid damping of turbulence, which cannot support clouds for a long time. This picture is supported by the turbulent structure of the clouds, as discussed below.

4. Observations of star-forming clouds such as ρ Ophiuchus show many prestellar clumps with masses around 0.1–0.3 $M_\odot$ (Motte, André, & Neri 1998; Bontemps et al. 2001), similar to the characteristic mass range determined in the present IMF calculations. Most interestingly, the mass spectrum of these clumps is quite similar to the IMF discussed in § 2 and thus quite similar to the young-star mass spectrum in the cloud, suggesting that the cloud stellar IMF derives directly from the clump mass spectrum. Similar results have been obtained in the Serpens cloud (Testi & Sargent 1998) and in Taurus (Onishi et al. 2002). This similarity of the IMF in prestellar condensation clouds and in isolated objects suggests that the general shape of the IMF is determined in the original gaseous phase and not during the collapse process during which the gas condenses into stars. This suggests that accretion cannot be the dominant mechanism of star formation. In other words, the initial conditions that determine the very star formation process most likely originate from large-scale processes that dissipate toward smaller scales. It also supports kind of a fragmentation characteristic mass scale such as the thermal Jeans mass, as discussed below. The large difference between the star and gas mass distribution derived from large-scale CO studies of molecular clouds, $N(m) \propto m^{-0.5}$ (see, e.g., Kramer et al. 1998), indicates the low efficiency in converting gas into stars. The rapid dispersal of molecular gas is likely to be one of the reasons for this low efficiency.

5. On large scales ($\gtrsim$pc), the spectral line widths observed in molecular clouds indicate highly supersonic motions (see, e.g., Falgarone, Puget, & Perault 1992), largely exceeding the thermal sound speed $c_S = (kT/\mu m_{\rm H})^{1/2} \approx 0.2$ km s^{-1} for $T = 10$ K ($\mu = 2.33$ is the mean molecular weight and $m_{\rm H}$ is the atomic mass unit). Moreover, the observations are consistent with super-Alfvénic conditions, with Alfvénic Mach numbers $\mathcal{M}_{\rm A}(L) = v/[B_0/(4\pi\rho_0)^{1/2}] \sim 10$, where ρ_0 denotes the gas density (Padoan & Nordlund 1999). These motions are thus believed to originate from large-scale supersonic and super-Alfvénic turbulence (Larson 1981, 1992; Elmegreen 1997; Padoan & Nordlund 1999). The observed line-width component σ obeys reasonably well the Larson (1981) relation $\sigma \sim 1$ km s^{-1} $(L/1\ {\rm pc})^{0.4}$ over a large-scale range 0.01 pc $< L <$ 100 pc (Falgarone et al. 1992). Dissipation of this nonthermal turbulent support on small scales ($\lesssim$0.1 pc) is prerequisite for the formation of prestellar cores (Nakano 1998). Note that the Larson scaling relation yields subsonic velocity dispersions at very small scales, consistent with the fact that even dense cluster-forming regions exhibit very narrow line widths for $\lesssim$0.1 pc, with a nonthermal to thermal velocity dispersion ratio of H_2 $\sigma_{\rm NT}/\sigma_T \sim 0.7$ (Belloche, André, & Motte 2001).

Star formation theories must now be compared with the general results (1–5). In a canonical theory for isolated star formation, low-mass stars form from the collapse of initially hydrostatic but unstable dense cloud cores that have reached a $\rho(r) \propto r^{-2}$ density distribution of a singular isothermal spheroid (Shu, Adams, & Lizano 1987). In this scenario, deuterium burning, which occurs at pre–main-sequence ages, is a key ingredient to trigger star formation. The onset of D-burning induces convective instability in the interior. Combined with the rapid rotation resulting from the accretion of angular momentum with mass, this convection is believed to generate a strong magnetic field through the dynamo process. The field will drive a magnetocentrifugal wind that ultimately sweeps away the surrounding accreting material and determines the mass of the nascent star. Within this picture, objects below the deuterium-burning limit cannot reverse the infall and thus cannot form gravitationally bound objects. Such a scenario can now be reasonably excluded on several grounds. First of all, substellar objects are fully convective, with or without deuterium burning, except for the oldest ones, which develop a conductive core at late ages (Chabrier & Baraffe 2000; Chabrier et al. 2000a). In fact, the numerous detections of free-floating objects at the limit and below the deuterium-burning minimum mass, and the rising mass spectrum down to this limit in several young clusters (see Fig. 5 and Najita et al. 2000; Béjar et al. 2001; Martín et al. 2001; Lucas et al. 2001), seem to exclude deuterium burning as a peculiar process in star formation. *This should close the ongoing debate in the literature arguing that the deuterium-burning minimum mass distinguishes BDs from planets, since such a distinction does not appear to be supported by physical considerations*. Second, as mentioned above, star formation in young clusters appear to form over a timescale significantly shorter than the ambipolar diffusion timescale $\gtrsim$10 Myr, indicating that, if magnetic field plays some role in star formation, it is unlikely to be a dominant process. In the ambipolar diffusion scenario, the cloud must survive long enough in near-equilibrium between magnetic and gravitational pressure. This is not consistent with observations of rapid star formation and cloud dissipation and with the observed turbulent nature of clouds. Indeed, equipartition between kinetic, gravitational, and magnetic energy fails to reproduce the observed properties of molecular clouds, which are dominated by super-Alfvénic and supersonic motions, where kinetic energy dominates magnetic energy with a decay timescale approximately equal to a dynamical timescale (see, e.g., Padoan & Nordlund 1999 and references therein). In fact, ambipolar diffusion models require large static magnetic field strengths (~30–100 μG) exceeding Zeeman estimates for low-mass dense cores ($\lesssim$10 μG)

(Crutcher & Troland 2000; Padoan & Nordlund 1999; Padoan et al. 2001a; Bourke et al. 2001).

Another version of the wind-limited accretion model relates the gas cloud properties (sound speed and angular velocity) to the stellar properties (mass and luminosity) through a direct relation between the accretion rate onto the star and the wind-driven mass-loss rate (Silk 1995; Adams & Fatuzzo 1996). However, it seems difficult in this model to explain the nearly universal shape of the IMF without sensitivity to the cloud parameters. More importantly, it appears rather difficult to produce free-floating gravitationally bound objects of brown dwarf and Jupiter masses in large numbers, since for too-small objects there will be no wind to stop accretion. Another argument against the wind limiting of the final core mass is that the observed outflows are relatively collimated, with opening angles less than 60°, making it difficult for these outflows to remove a large fraction of the protostellar core. Therefore, although wind regulation might play some role in determining the final object mass, in particular for large masses, it is unlikely to play a dominant role in star formation.

An alternative process to determine the final stellar mass is opacity-limited fragmentation (Hoyle 1953; Larson 1969; Silk 1977). In this model, the protostellar cloud keeps fragmenting under the action of gravity until it becomes optically thick and can no longer cool. Coincidentally, this characteristic minimum mass for the low-temperature chemically enriched conditions prevailing in today's molecular clouds is similar to the deuterium-burning minimum mass, namely, $\sim 0.01\ M_\odot$ (Silk 1977; Larson 1992). In this scenario, one might expect an accumulation of objects near this characteristic mass, from which more massive objects will grow. The rather smooth continuation of the stellar and substellar MF down to this mass scale, although still subject to large uncertainties, seems to exclude such an accumulation.

In fact, all these scenarios enter more or less the general models of hierarchical fragmentation, based on a Jeans formulation, where the fragmentation process is determined essentially by comparing the effective isothermal sound crossing time $\sim L/T^{1/2}$ and the free-fall time $\sim \rho^{-1/2}$, and where the physical process that initiates the gravitational collapse is generally believed to be gravity, yielding a formation process determined by the local gravitational timescale $(G\rho)^{-1/2}$ (Larson 1978; Elmegreen 1997, 1999). However, all substellar objects have a mass significantly smaller than any Jeans mass. This suggests that gravity is not the determinant mechanism that triggers star formation and shapes the clumps in the initial molecular clouds. Gravity more likely amplifies the existing density fluctuations but does not create them. The observational data thus seem to exclude gravitational fragmentation as the *dominant* process that determines the characteristic mass distribution for star formation. Moreover, in the models of Jeans instability driven star formation, the thermal energy of the cloud must be comparable to its gravitational content. As mentioned above, however, turbulent kinetic energy in star-forming clouds supersedes thermal energy by about a factor of ~100. Redefining the Jeans scenario in terms of turbulent kinetic energy is flawed because compressible turbulence dissipates in fragmenting the gas in filaments, i.e., in a highly nonhomogeneous manner. Furthermore, turbulence is a highly nonlinear process, opposite to the basic assumption of the gravitational instability model.

Alternative models suggested that stars grow from protostar collisions and/or coalescence between gas clumps until the bound fragment becomes optically thick (Nakano 1966; Nakano, Hasegawa, & Norman 1995). The aforementioned rapid timescale for star formation, however, is much shorter than the typical collision time between multiple protostellar clumps and thus seems to exclude this scenario, at least for the low-mass stars. It is also difficult to reconcile this star formation mechanism, involving kind of feedback effects, with the universal form of the IMF, suggesting that the latter reflects the initial conditions imposed in the cloud, not to mention the difficulty in reconciling coalescence processes with supersonic turbulence. A recent extension of this type of scenario, where the IMF is determined by the competitive accretion between the various stellar cores and a combination of mass accretion and stellar mergers, has been proposed by Bonnel, Bate, and collaborators (Bonnell et al. 2001a, 2001b; Bonnell & Bate 2002), on the basis of hydrodynamical simulations of gas accretion onto a preexisting cluster of 1000 stars. Based on 15 stars with $m \gtrsim 5\ M_\odot$ at the end of the calculations, the high-mass tail of the IMF obtained with such an accretion and merger scenario seems to reproduce a Salpeter slope, although the reason for such a result is not clear, whereas the lower mass part of the IMF yields a shallower power law with $x \approx 0.5$. Although, as mentioned earlier, the accretion process certainly plays some role in shaping the final stellar mass, the present scenario relies on some assumptions for the initial conditions, e.g., an ensemble of already formed stars of equal mass as nucleation centers and a gas reservoir apparently not supersonic, which appear rather unrealistic.

Finally, some models suggest that star formation is not due to a dominant process but is rather the by-product of several independent processes of comparable importance. The product of a large number of statistically independent processes naturally points to the central limit theorem, as initially suggested by Larson (1973), Zinnecker (1984), and Elmegreen (1985), and later by Adams & Fatuzzo (1996). The final product of the central limit theorem is a Gaussian distribution, i.e., a log-normal form in a logarithmic plane. In this type of theory, however, the statistical aspect of star formation still arises from the hierarchical structure produced by fragmentation and thus is linked back to the original concept of Hoyle. Moreover, this theory is frustrating from the physics point of view, since it relies on a purely statistical mechanism and prevents understanding star formation from identified physical processes, not to mention delicate applications of the central limit theorem concept, which strictly speaking implies an *infinity* of statistically independent variables, in real nature! In fact, no current

theory of the IMF is consistent with all the aforementioned constraints (1–5) and predicts in particular the formation of free-floating objects in significant numbers at very low mass.

A picture of star formation driven by compressible turbulence has been suggested recently by various independent approaches (Padoan & Nordlund 1999; Klessen 2001; Bate, Bonnell, & Bromm 2002, 2003; see Nordlund & Padoan 2002 and Mac Low & Klessen 2003 for recent reviews). Although these approaches use different methods and differ on the details of the interplay between turbulence and gravity, they are similar in spirit and share the same underlying dominant idea: star formation is generated initially by the (inhomogeneous) dissipation of supersonic turbulence, forming dense cores in which eventually gravity becomes important enough for the cores to become unstable and form gravitationally bound objects. A comprehensive picture of such a star formation mechanism, in super-Alfvénic conditions, has been derived recently by Nordlund & Padoan and is summarized below (see Nordlund & Padoan 2002).

The power spectrum of turbulence on a large scale L in the inertial range (below the energy injection scale and above the dissipation scale) is a power law

$$E(k) \propto k^{-\beta}, \tag{28}$$

where $k = 2\pi/\lambda$ is the wavenumber and λ is the dynamical scale of turbulence. Recent numerical simulations of compressible turbulence in a magnetized gas (Boldyrev, Nordlund, & Padoan 2002a, 2002b; Padoan et al. 2003b) yield a power spectrum consistent with $\beta = 1.74$, between incompressible turbulence $\beta \approx 5/3$ (Kolmogorov spectrum) and pressureless turbulence $\beta \approx 2$ (Burgers 1974). The rms velocity σ on the scale L of the gas extension before the shock is related to this power spectrum index by $\sigma^2 \propto L^{\beta-1} \Rightarrow \sigma \propto L^{(\beta-1)/2=\alpha} \sim L^{0.37}$, which agrees quite well with the aforementioned observed σ-L Larson's relation. In these simulations, the upstream Alfvénic Mach number $\mathcal{M}_A(L)$ is assumed to follow a Larson-type relation, i.e., to scale as L^α, where $\alpha = (\beta - 1)/2 \approx 0.4$ from above. A second assumption is that self-similarity holds at different scales, so that the number of cores in the shocked gas scales with the size L of the upstream flows out of which they formed, $N \sim L^{-3}$.

This spectrum, completed by the jump conditions for isothermal MHD shocks, $\rho/\rho_0 \approx L/l \approx B/B_0 \approx \mathcal{M}_A$—where ρ_0, B_0, and L denote the gas density, magnetic field strength, and gas extension before the shock, respectively, while l denotes the size of the cores in the shocked gas, and the quantities without indices refer to the postshock situation—and by the aforementioned scaling relations for the number of dense cores $N(m)$ of mass m formed in the shocked (filamentary) gas, yields a mass distribution of dense cores (Padoan & Nordlund 2002),

$$N(m)d\log m \propto m^{-3/(4-\beta)}d\log m \propto m^{-1.33}d\log m, \tag{29}$$

similar to the Salpeter value.

In these simulations, the typical core mass formed in shocked gas reads

$$m(L) \sim \rho l^3 \sim \rho_0 L^3/\mathcal{M}_A(L)^2 \sim L^{3-2\alpha} \sim L^{2.2}. \tag{30}$$

In this turbulent picture of fragmentation, the distribution of cores arises essentially from internal cloud turbulent dissipation. The collapse of these cores into protostars is then determined by the dynamical timescale of supersonic MHD turbulence $\tau_{\rm dyn} = L/\sigma(L)$ rather than by the local gravitational timescale $(G\rho)^{-1/2}$. Sufficiently massive cores continue to collapse under self-gravity, so for large m, the distribution of cores is directly reflected in the distribution of stellar masses. At smaller masses, only cores with sufficient density are able to collapse further, which reduces the number of stars formed out of a given distribution of cores with mass m and causes the IMF to deviate from the large-m behavior. Thus, in a generic sense, the rollover of the IMF happens when gravity is no longer able to cause the collapse of most cores of a given mass. At this stage, different factors such as cooling functions, equations of state, additional fragmentation during collapse, etc., become important. Quantitative predictions then require detailed numerical simulations, such as those of Bate et al. (2002, 2003) or Klessen (2001). If, for example, because of gravitational fragmentation during the collapse, each core gives rise to a distribution of stars, the IMF will be shifted to smaller masses. This will not influence the power-law shape on the high-mass side but will shift the maximum mass of the IMF to a smaller value, affecting the expected number of low-mass stars and brown dwarfs.

Qualitatively, however, the rollover of the IMF is displayed already for idealized assumptions with isothermal conditions. A universal behavior of turbulent fragmentation for an isothermal gas is that it produces a lognormal probability distribution function (PDF) of gas density in unit of mean density $x = n/n_0$:

$$p(x)d\ln x \propto \exp\left[-\frac{(\ln x - \langle \ln x\rangle)^2}{2\sigma^2}\right] d\ln x, \tag{31}$$

where n_0 is the mean density and $\sigma^2 \approx \ln(1 + 0.25\mathcal{M}^2)$ (Padoan, Nordlund, & Jones 1997; Padoan & Nordlund 1999; Ostriker, Gammie, & Stone 1999). In the present context of star formation, this no longer yields a unique Jeans mass but a distribution of local Jeans masses $p(m_J)$, obtained from the PDF of gas density, assuming that the distribution of average density of clumps of a given mass also has a lognormal distribution (Padoan et al. 1997, 2001b; Padoan & Nordlund

2002):

$$p(m_J)\, d\ln m_J = \frac{2}{\sqrt{2\pi\sigma}}\, m_J^{-2} \exp\left[-\frac{(\ln m_J^2 - |\langle \ln x\rangle|)^2}{2\sigma^2}\right] d\ln m_J, \tag{32}$$

where m_J is written in units of the thermal Jeans mass at mean density n_0:

$$M_J = 1.2\, M_\odot \left(\frac{T}{10\ \mathrm{K}}\right)^{3/2} \left(\frac{n_0}{10^4\ \mathrm{cm}^{-3}}\right)^{-1/2}$$
$$= 1.2\, M_\odot \left(\frac{T}{10\ \mathrm{K}}\right)^{2} \left(\frac{P_0}{10^5\ \mathrm{cm}^{-3}\ \mathrm{K}}\right)^{-1/2}, \tag{33}$$

which thus ranges from ~1.2 to ~0.12 $M_\odot$ for characteristic low-pressure to high-pressure clumps.[14] The Jeans mass is approximately the same for spheres and for filaments (Larson 1985).

The fraction of small cores of mass $m < M_J$ to collapse to gravitationally bound structures is thus given by the probability distribution $P(m) = \int_0^m p(m_J)\, dm_J$, and the mass distribution of collapsing cores reads (from eq. [29])

$$N(m)\, d\ln m \propto m^{-3/(4-\beta)} P(m)\, d\ln m. \tag{34}$$

Therefore, although the *average* star mass is similar to the average thermal Jeans mass of the medium, the global mass distribution extends well below this limit, with decreasing probability. Within this picture, star formation proceeds as follows (see Nordlund & Padoan 2002):

1. Supersonic turbulence in the ISM, produced by large amounts of kinetic energy at large scales, dissipates in fragmenting molecular clouds (preventing a global collapse of the cloud) into highly anisotropic filaments, as a result of the random convergence of the velocity field. These filaments form dense cores with large density contrasts (much larger than the maximum value ~14 for a self-gravitating, pressure-bounded Bonnor-Ebert sphere) via the action of radiative MHD shocks and thus determine the fragmentation length scale over which collapse is possible. Cooling becomes more efficient as density increases in these dense cores, of typical dimensions ~0.01–0.1 pc, which become self-gravitating and begin to collapse. During this stage, the star formation process itself, during which gas is converted into stars, plays no particular role. Star formation arises essentially from dissipation of supersonic turbulence toward small scales in molecular clouds, since there is no dissipation mechanism at large scales. This turbulent dissipation yields a universal power spectrum and is thus independent of the local conditions in the star-forming clouds, a result supported by the observations. The main source of kinetic energy in the cloud is supplied by large-scale motions, which produce the turbulent cascade. The initial cloud structure is not essential, except possibly for the initial amount of available turbulent energy in the cloud, because of the universal character of turbulent structures in various environments.

2. The small-scale dissipation of this large-scale turbulence follows the Larson (1981) relation, yielding subsonic structures ($\lesssim$0.1 km s^{-1}) at small scales ($\lesssim$0.1 pc) typical of protostellar cores. While this process is scale free for scales largely above the minimum Jeans scale, generating a power-law tail, a characteristic mass enters at small scale, namely, the minimum mass for gravitational binding energy to exceed mostly the thermal, and to a lesser extent the magnetic energy, i.e., the Jeans mass (or more exactly the Bonnor-Ebert mass). Since fragmentation is driven by supersonic turbulence, however, star-forming clumps can no longer be regarded as equilibrium configurations, and the concept of a unique thermal Jeans mass no longer applies. Indeed, there is a *distribution* of local Jeans masses determined by the (lognormal) probability distribution function of gas density set up by turbulent fragmentation. Objects below this mass scale form with a rapidly decreasing (but not zero) probability with decreasing core mass, since they come from the exponential tails of the density and Mach number distributions. It should be noted that turbulence in protostellar clouds indeed appears to generate structures much smaller than the thermal Jeans mass, down to ~10^{-4} $M_\odot$ (Langer et al. 1995; Heithausen et al. 1998; Kramer et al. 1998), suggesting that a fragmentation mechanism other than a purely Jeans gravitational instability may play an important role for the dynamics of these dense structures.

In this scenario, other processes such as gravitational or opacity-limited fragmentation, protostar interactions, and stellar winds or accretion, although playing some role in determining the final stellar mass distribution, e.g., by limiting the efficiency of star formation, appear to be of secondary importance; the triggering process of star formation is small-scale dissipation of compressible turbulence, which forms cores. Then, *self-gravity drives the subsequent collapse and star formation*. The turbulent structure of the parent cloud can be maintained either by the young stars, which, because of the short timescale of star formation, do not have time to move far away from their birth site and reinject kinetic energy into the ISM through outflows, by supernovae, or by galactic shear. In fact, given the short timescale for star formation, turbulent energy does not have to be resupplied constantly, and cloud dissipation may occur within the star formation timescale (Elmegreen 2000). Note that the turbulent nature of the cloud also provides a natural explanation for the low efficiency of star formation, besides rapid dissipation of the cloud itself. Indeed, star for-

[14] Note the incorrect density scaling factor, 10^3 cm^{-3}, in Padoan & Nordlund (2002, eq. [21]) (Å. Nordlund 2002, private communication). Using the same expression for the Jeans mass as Bonnell et al. (2001a, eq. [1]), the scaling constant changes from 1.2 to 1.9 $M_\odot$

mation occurs only in some high-density regions of the filament intersections, and most molecular gas resides either in the low-density interclump regions or in the dense regions too small to become self-gravitating (Padoan 1995). Interestingly enough, the problem of stopping accretion on the collapsing protostar does not really arise in this picture, for the protostar mass is essentially defined by the finite amount of mass available in the corresponding core mass. Rotation is another important issue. Indeed, although rotational energy in cores ($\Omega_{\rm rot} \sim 10^{-14}$ rad s^{-1}) represents about 1%–2% of the gravitational energy, the core must get rid of its angular momentum. The detailed simulations of Abel, Bryan, & Norman (2002), however, indicate that a core does get rid of angular momentum sufficiently efficiently to give rise to a single star, most of the angular momentum being transported by the shock waves during the turbulent collapse.

Providing large enough density in the initial cloud (or conversely large enough Mach number for a given density), the mass spectrum obtained by these calculations extends well into the BD domain (Padoan & Nordlund 2002; Padoan et al. 2001b; Nordlund & Padoan 2002). This provides a natural explanation for the formation of BDs, suggesting that BDs form from the same general IMF produced by the cloud collapse as the stars. This is consistent with the results presented in § 2, which show that the observed population of BDs in the Galactic field is well reproduced by the same underlying IMF as in the stellar regime (see also Chabrier 2002). This seems to disfavor the scenario of BD formation produced by violent dynamical ejection of small embryos from the collapsing cloud (Reipurth & Clarke 2001; Bate et al. 2002, 2003) as the *dominant* formation process for these objects. Such a scenario raises also other problems including the BD radial velocity dispersion, binary frequency, and circumstellar properties (see, e.g., Joergens & Guenther 2001; Bate et al. 2003; Close et al. 2003; White & Basri 2003). Competition between collision and interrupted accretion (Bate et al. 2002), the detailed fragmentation distribution in the collapse from cores to objects (Klessen 2001), and the multiplicity distribution, however, can contribute to extending the IMF toward smaller scales and need to be quantified by detailed numerical simulations.

As mentioned earlier, the initial density of the parent cloud, as well as the initial level of turbulence, is important in determining the amount of objects well below the thermal Jeans mass, in particular in the BD regime. Nordlund & Padoan (2002) find that reducing the density of the cloud by a factor of 5, or reducing the Alfvénic Mach number on a 10 pc size by a factor of 2, reduces the number of BDs by about a factor of 10. We had already noted that the fraction of substellar over stellar objects in Taurus ($n \sim 1$ pc^{-3}) is about a factor of 2 smaller than in other young clusters (Briceño et al. 2002). The initial amount of turbulence also leads to significant differences at intermediate scales (~0.1 pc) between the line widths observed in regions of isolated star formation such as Taurus, which is dominated by thermal motions ($\sigma \lesssim 0.2$ km s$^{-1} \sim c_S$), and the ones observed in dense cluster-forming cores ($n \gtrsim 10^3$ pc^{-3}), such as, e.g., Ophiuchus or Orion, which are dominated by turbulent motions. In fact, protostellar clouds in Taurus, with size ~0.1 pc, exhibit properties different from the ones observed in denser cluster-forming regions and seem to be consistent with the standard Shu et al. (1987) quasi-static isothermal collapse scenario (Motte & André 2001). If confirmed in other clouds of similar density, these results may indicate that star formation in low-density environments, representative of isolated mode of star formation, differs from star formation in denser clouds, representative of cluster-forming star formation, which is the dominant mode of star formation (see, e.g., Myers 1998). These results imply that star formation of low-mass objects depends to some extent on the environment (1) from the initial amount of kinetic energy imprinted by turbulence and (2) because of some density threshold that separates two dominant mechanisms. In dense regions above the threshold, star formation is dominated by dissipation of compressible turbulence, whereas in regions below the threshold density, where the amount of turbulence is smaller, stars form in isolation and obey the standard isothermal gravitational collapse scenario. As noted previously, however, the timescale for star formation in these regions is much shorter than the one predicted by ambipolar diffusion (Fig. 11), implying that even in low-density star formation regions, the initial collapse is triggered by large-scale turbulent dissipation, but the final cores are formed essentially by (dynamic) gravitational fragmentation in subsonic flows (see, e.g., Hartmann 2002; Padoan et al. 2003a). Given the lower density in these regions, we expect a larger mean thermal Jeans mass than in denser regions, since $M_{\rm J} \propto \rho^{-1/2}$, and thus a deficit of very low mass and substellar objects.

8. SUMMARY AND CONCLUSIONS

In this review, we have examined recent determinations of the IMF in various components of the Galaxy: disk, spheroid, young, and globular clusters. Based on the most recent observations and state-of-the-art evolutionary models for low-mass stars and brown dwarfs, we have determined the PDMF and IMF in these different environments. As a general feature, we find that the IMF depends weakly on the environment and is well described by a power-law form at $m \gtrsim 1\ M_\odot$ and a log-normal form below this limit. The disk IMF, for isolated objects, has a characteristic mass around ~0.1 $M_\odot$ and a variance in logarithmic mass $\sigma \sim 0.7$, whereas the disk IMF for multiple systems has a characteristic mass ~0.2 $M_\odot$ and a variance $\sigma \sim 0.6$. These disk single and system MFs are consistent with a binary fraction among low-mass stars ~50%, implying a fraction ~20% of BD companions of M dwarfs, in agreement with present determinations. The results are consistent with masses for the singles, primaries, and companions drawn randomly from the same underlying single IMF or similarly from a more or less uniform mass ratio distribution. The extension of the single MF into the BD regime is in good agreement with

present estimates of L- and T-dwarf densities, when considering all the uncertainties in these estimates. This yields a disk BD number density comparable to the stellar one, namely, ~ 0.1 pc^{-3}. The IMF of several young clusters is found to be consistent with this same field IMF, providing a similar correction for unresolved binaries, confirming the fact that young star clusters and disk field stars represent the same stellar population. Dynamical effects, yielding depletion of the lowest mass objects, are found to become consequential for ages slightly older than the age of the Pleiades, i.e., $\gtrsim$130 Myr.

The spheroid IMF relies on much less robust grounds. The large metallicity spread in the photometric local sample, in particular, remains puzzling. Recent observations suggest that there is a continuous kinematic shear between the thick-disk population present in the local samples and the spheroid one observed with *HST*. This enables us to derive only an upper limit for the spheroid mass contribution and IMF. The latter is found to be similar to the one derived for globular clusters and is well described also by a lognormal form, but with a characteristic mass slightly larger than for the disk, around $\sim$0.2–0.3 $M_{\odot}$. Such an IMF excludes a significant population of BDs in globular clusters and in the spheroid, i.e., in metal-depleted environments. These results, however, remain hampered by large uncertainties such as the exact amount of dynamical evolution near the half-mass radius of a globular cluster, the exact identification of the genuine spheroid population, and the exact fraction of binaries in globular cluster and spheroid populations.

The early-star IMF, representative of stellar populations formed at large redshift ($z \gtrsim 5$), remains undetermined, but different observational constraints suggest that it does not extend below $\sim 1\ M_{\odot}$. Whether it extends down to this mass range, implying the existence of a primordial white dwarf population, or whether the cutoff for this primordial IMF occurs at much larger masses remains unsettled. In any case, the baryonic content of the dark halo represents very likely at most a few percent of the Galactic dark matter.

These determinations point to a characteristic mass for star formation that decreases with time, from early star formation conditions of temperature and metallicity, to conditions characteristic of the spheroid or thick-disk environments, to present-day conditions. These results, however, remain more suggestive than conclusive. These IMFs allow a reasonably robust determination of the Galactic stellar and brown dwarf content. They have also important galactic implications beyond the Milky Way in yielding more accurate mass-to-light ratio determinations. The IMFs determined for the disk and the spheroid yield mass-to-light ratios a factor of 1.8–1.4 smaller than for a Salpeter IMF, respectively, in agreement with various recent dynamical determinations.

This IMF determination is examined in the context of star formation theory. Theories based on a pure Jeans-type mechanism, where fragmentation is due only to gravity, appear to have difficulties explaining the determined IMF and various observational constraints on star formation. On the other hand, recent numerical simulations of compressible turbulence, in particular in super-Alfvénic conditions, reproduce qualitatively and reasonably quantitatively the determined IMF and thus provide an appealing solution. In this picture, star formation is induced by the dissipation of large-scale turbulence to smaller scales through radiative shocks, producing filamentary structures. These shocks produce local, nonequilibrium structures with large density contrasts. Some of these dense cores then collapse eventually in gravitationally bound objects under the combined action of turbulence and gravity. The concept of a single Jeans mass, however, is replaced by a distribution of local Jeans masses, representative of the lognormal probability density function of the turbulent gas. Cores exceeding the average Jeans mass ($\gtrsim 1\ M_{\odot}$) naturally collapse into stars under the action of gravity, whereas objects below this limit still have a possibility to collapse, but with a decreasing probability, as gravity selects only the densest cores in a certain mass range (the ones such that the mass exceeds the local Jeans mass m_J). This picture, combining turbulence as the initial mechanism for fragmentation and gravity, thus provides a natural explanation for a scale-free power-law IMF at large scales and a broad lognormal form below about 1 $M_{\odot}$. Additional mechanisms such as accretion, subfragmentation of the cores, and multiplicity will not significantly affect the high-mass power-law part of the mass spectrum but can modify the extension of its low-mass part. The initial level of turbulence in the cloud and its initial density can also affect the low-mass part of the IMF.

Future improvements on both the theoretical and observational sides should confirm (or refute) this general scenario and help quantify the details of the interaction between turbulence and gravity, but it is encouraging to see that we are now reaching a reasonable paradigm in our understanding of the Galactic mass function over 5 orders of magnitude, from very massive stars to Jupiter-like objects; of the census of baryonic objects in the Galaxy, which can be applied to external galaxies; and of the dominant physical mechanisms underlying the process of star formation.

It is a great pleasure for me to thank many colleagues who contributed to this review. Special thanks to D. Barrado y Navascues, V. Béjar, J. Bouvier, A. Burgasser, F. Comerón, C. Dahn, P. Dobbie, N. Hambly, H. Harris, D. Kirkpatrick, K. Luhman, and E. Moraux for sending their data and in some cases sharing unpublished results. My profound gratitude goes to S. Charlot for calculating the mass-to-light ratios in § 6. Finally, I am deeply indebted to I. Baraffe, J. Bouvier, G. DeMarchi, L. Hartmann, P. Kroupa, R. Larson, and Å. Nordlund for numerous discussions and highly valuable comments and for reading a preliminary version of this review. Finally, special thanks to Anne Cowley and David Hartwick, editors of *PASP*, for their astronomical patience before they received the present manuscript.

REFERENCES

Abel, T., Bryan, G. L., & Norman, M. L. 2000, ApJ, 540, 39
———. 2002, Science, 295, 93
Adams, F., & Fatuzzo, M. 1996, ApJ, 464, 256
Adams, F., & Laughlin, G. 1996, ApJ, 468, 586
Adams, J., Stauffer, J., Monet, D., Skrutskie, M., & Beichman, C. 2001, AJ, 121, 2053
Afonso, C., et al. (EROS Collaboration). 2003, A&A, 400, 951
Albrow, M. D., Gilliland, R. L., Brown, T. M., Edmonds, P. D., Guhathakurta, P., & Sarajedini, A. 2001, ApJ, 559, 1060
Alcock, C., et al. (MACHO Collaboration). 2000, ApJ, 542, 281
Bahcall, J., & Casertano, S. 1986, ApJ, 308, 347 (BC86)
Bahcall, J., Flynn, C., Gould, A., & Kirhakos, S. 1994, ApJ, 435, L51
Baraffe, I., Chabrier, G., Allard, F., & Hauschildt, P. H. 1997, A&A, 327, 1054 (BCAH97)
———. 1998, A&A, 337, 403 (BCAH98)
———. 2002, A&A, 382, 563
———. 2003, in IAU Colloq. 211, Brown Dwarfs, ed. E. Martín (San Francisco: ASP), in press
Barrado y Navascues, D., Bouvier, J., Stauffer, J. R., Lodieu, N., & McCaughrean, M. J. 2002, A&A, 395, 813
Bate, M. R., Bonnell, I. A., & Bromm, V. 2002, MNRAS, 332, L65
———. 2003, MNRAS, 339, 577
Baumgardt, H., & Makino, J. 2003, MNRAS, 340, 227
Bedin, L., Anderson, J., King, I., & Piotto, G. 2001, ApJ, 560, L75
Béjar, V., et al. 2001, ApJ, 556, 830
Belloche, A., André, P., & Motte, F. 2001, in ASP Conf. Ser. 243, From Darkness to Light, ed. T. Montmerle & Ph. André (San Francisco: ASP), 313
Blain, A. W., Smail, I., Ivison, R. J., & Kneib, J.-P. 1999, MNRAS, 302, 632
Boldyrev, S., Nordlund, Å., & Padoan, P. 2002a, ApJ, 573, 678
———. 2002b, Phys. Rev. Lett., 89, 1102
Bonnell, I. A., & Bate, M. 2002, MNRAS, 336, 659
Bonnell, I. A., Bate, M., Clarke, C., & Pringle, J. 2001a, MNRAS, 323, 785
Bonnell, I. A., Clarke, C., Bate, M., & Pringle, J. 2001b, MNRAS, 324, 573
Bontemps, S., et al. 2001, A&A, 372, 173
Bourke, T., Myers, P., Robinson, G., & Hyland, A. 2001, ApJ, 554, 916
Briceño, C., Luhman, K. L., Hartmann, L., Stauffer, J. R., & Kirkpatrick, J. D. 2002, ApJ, 580, 317
Bromm, V., Coppi, P., & Larson, R. B. 2002, ApJ, 564, 23
Burgasser, A. J. 2001, Ph.D. thesis, Caltech
Burgasser, A. J., Kirkpatrick, J. D., Reid, I. N., Brown, M., Miskey, C., & Gizis, J. 2003, ApJ, 586, 512
Burgers, J. M. 1974, The Nonlinear Diffusion Equation (Dordrecht: Reidel)
Casertano, S., Ratnatunga, K., & Bahcall, J. 1990, ApJ, 357, 435
Cen, R. 2003, ApJ, submitted
Chabrier, G. 1999, ApJ, 513, L103
———. 2001, ApJ, 554, 1274
———. 2002, ApJ, 567, 304
———. 2003, ApJ, 586, L133
Chabrier, G., & Baraffe, I. 1997, A&A, 327, 1039
———. 2000, ARA&A, 38, 337
Chabrier, G., Baraffe, I., Allard, F., & Hauschildt, P. H. 2000a, ApJ, 542, 464
———. 2000b, ApJ, 542, L119
Chabrier, G., & Méra, D. 1997, A&A, 328, 83
Chabrier, G., Segretain, L., & Méra, D. 1996, ApJ, 468, L21
Christlieb, N., et al. 2002, Nature, 419, 904
Ciardi, B., Ferrara, A., & White, S. D. M. 2003, MNRAS, submitted
Ciolek, G. E., & Mouschovias, T. Ch. 1995, ApJ, 454, 194
Close, L., Siegler, N., Freed, M., & Biller, B. 2003, ApJ, 587, 407
Comerón, F., Fernández, M., Baraffe, I., Neuhäuser, R., & Kaas, A. A. 2003, A&A, in press
Crucher, R., & Troland, T. 2000, ApJ, 537, L139
Dahn, C. C., Liebert, J., & Harrington, R. S. 1986, AJ, 91, 621
Dahn, C. C., Liebert, J., Harris, H. C., & Guetter, H. H. 1995, in Proc. ESO Astrophys. Symp., The Bottom of the Main Sequence and Beyond, ed. C. Tinney (Berlin: Springer), 239
de la Fuente Marcos, C., & de la Fuente Marcos, R. 2000, Ap&SS, 271, 127
Delfosse, X., Forveille, T., Ségransan, D., Beuzit, J. L., Udry, S., Perrier, C., & Mayor, M. 2000, A&A, 364, 217
De Marchi, G., Leibundgut, B., Paresce, F., & Pulone, L. 1999, A&A, 343, L9
De Marchi, G., Paresce, F., & Pulone, L. 2000, ApJ, 530, 342
Digby, A. P., Hambly, N. C., Cooke, J. A., Reid, I. N., & Cannon, R. D. 2003, MNRAS, in press (astro-ph/0304056)
Dobbie, P., Kenyon, F., Jameson, R., Hodgkin, S., Hambly, N., & Hawkins, M. 2002a, MNRAS, 329, 543
Dobbie, P., Kenyon, F., Jameson, R., Hodgkin, S., Pinfield, S., & Osborne, S. 2002b, MNRAS, 335, 687
Dobbie, P., Pinfield, D., Jameson, R., & Hodgkin, S. 2002c, MNRAS, 335, L79
Dwek, E., et al. 1998, ApJ, 508, 106
Eggen, O. J. 1979, ApJS, 39, 89
———. 1980, ApJS, 43, 457
Elmegreen, B. G. 1985, in Les Houches, Session XLI, Birth and Infancy of Stars, ed. R. Lucas, A. Omont, & R. Stora (Amsterdam: Elsevier), 257
———. 1997, ApJ, 486, 944
———. 1999, ApJ, 515, 323
———. 2000, ApJ, 530, 277
Elson, R., Santiago, B., & Gilmore, G. 1996, NewA, 1, 1
ESA. 1997, The *Hipparcos* and Tycho Catalogues (ESA SP-1200; Noordwijk: ESA)
Falgarone, E., Puget, J.-L., & Perault, M. 1992, A&A, 257, 715
Fall, M., & Rees, M. 1985, ApJ, 298, 18
Feigelson, E. D. 1996, ApJ, 468, 306
Fields, B., Freese, K., & Graff, D. 2000, ApJ, 534, 265
Fuchs, B., & Jahreiss, H. 1998, A&A, 329, 81
Fuchs, B., Jahreiss, H., & Wielen, 1999, Ap&SS, 265, 175
Fuhrmann, K. 2002, NewA, 7, 161
Fujimoto, M. Y., Ikeda, Y., & Iben, I., Jr. 2000, ApJ, 529, L25
Gibson, B., & Mould, J. 1997, ApJ, 482, 98
Gilmore, G., & Reid, N. 1983, MNRAS, 202, 1025
Gilmore, G., Wyse, R. F. G., & Norris, J. E. 2002, ApJ, 574, L39
Gizis, J. E., Kirkpatrick, J. D., Burgasser, A. J., Reid, I. N., Monet, D. G., Liebert, J., & Williams, R. J. 2001, ApJ, 551, L163
Gizis, J. E., Monet, D., Reid, I. N., Kirkpatrick, J. D., Liebert, J., & Wilson, J. C. 2000, AJ, 120, 1085
Gizis, J. E., & Reid, I. N. 1999, AJ, 117, 508
———. 2000, PASP, 112, 610
Gizis, J. E., Reid, I. N., & Monet, D. 1999, AJ, 118, 997
Gnedin, N. Y., & Ostriker, J. 1997, ApJ, 486, 581
Gould, A. 2003, ApJ, 583, 765
Gould, A., Bahcall, J. N., & Flynn, C. 1997, ApJ, 482, 913 (GBF97)
Gould, A., Flynn, C., & Bahcall, J. N. 1998, ApJ, 503, 798 (GFB98)

Gould, A., & Popowski, P. 1998, ApJ, 508, 844
Graff, D., & Freese, K. 1996, ApJ, 456, L49
Groenewegen, M. A. T., et al. 2002, A&A, 392, 741
Halbwachs, J.-L., Arenou, F., Mayor, M., Udry, S., & Queloz, D. 2000, A&A, 355, 581
Hambly, N. C., Hodgkin, S. T., Cossburn, M. R., & Jameson, R. F. 1999, MNRAS, 303, 835
Hartmann, L. 2001, AJ, 121, 1030
———. 2002, ApJ, 578, 914
———. 2003, ApJ, 585, 398
Hartmann, L., Calvet, P., Gullbring, N., & D'Alessio, P. 1998, ApJ, 495, 385
Hartmann, L., Cassen, P., & Kenyon, S. 1997, ApJ, 475, 770
Hauser, M. G., & Dwek, E. 2001, ARA&A, 39, 249
Haywood, M., Robin, A., & Crézé, M. 1997, A&A, 320, 440
Heithausen, A., Bensch, F., Stutzki, J., Falgarone, E., & Panis, J.-F. 1998, A&A, 331, L65
Henry, T. J., Franz, O. G., Wasserman, L. H., Benedict, G. F., Shelus, P. J., Ianna, P. A., Kirkpatrick, J. D., & McCarthy, D. W., Jr. 1999, ApJ, 512, 864
Henry, T. J., Ianna, P. A., Kirkpatrick, D., & Jahreiss, H. 1997, AJ, 114, 388
Henry, T. J., & McCarthy, D. W. 1990, ApJ, 350, 334
———. 1993, AJ, 106, 773
Holberg, J. B., Oswalt, T. D., & Sion, E. M. 2002, ApJ, 571, 512
Hoyle, F. 1953, ApJ, 118, 513
Joergens, V., & Guenther, E. 2001, A&A, 379, L9
Jorissen, A., Mayor, M., & Udry, S. 2001, A&A, 379, 992
Kennicutt, R. C., Tamblyn, P., & Congdon, C. W. 1994, ApJ, 435, 22
Kenyon, S. J., & Hartmann, L. 1990, ApJ, 349, 197
King, I., Anderson, J., Cool, A., & Piotto, G. 1998, ApJ, 492, L37
Kirkpatrick, J. D., et al. 1999, ApJ, 519, 802
———. 2000, AJ, 120, 447
Klessen, R. 2001, ApJ, 556, 837
Kramer, C., Stutzki, J., Röhrig, R., & Corneliussen, U. 1998, A&A, 329, 249
Kroupa, P. 1995, ApJ, 453, 350
———. 2001, MNRAS, 322, 231
———. 2002, Science, 295, 82
Kroupa, P., Aarseth, S., & Hurley, J. 2001, MNRAS, 321, 699
Kroupa, P., Tout, C. A., & Gilmore, G. 1991, MNRAS, 251, 293
———. 1993, MNRAS, 262, 545
Langer, W., Velusamy, T., Kuiper, T., Levin, S., Olsen, E., & Migenes, V. 1995, ApJ, 453, 293
Larson, R. 1969, MNRAS, 145, 271
———. 1973, MNRAS, 161, 133
———. 1978, MNRAS, 184, 69
———. 1981, MNRAS, 194, 809
———. 1985, MNRAS, 214, 379
———. 1992, MNRAS, 256, 641
———. 1998, MNRAS, 301, 569
Leggett, S., Allard, F., Berriman, G., Dahn, C. C., & Hauschildt, P. H. 1996, ApJS, 104, 117
Lilly, S. J., Le Fèvre, O., Hammer, F., & Crampton, D. 1996, ApJ, 460, L1
Lu, L., Sargent, W., Churchill, C., & Vogt, S. 1996, ApJS, 107, 475
Lucas, P. W., Roche, P. F., Allard, F., & Hauschildt, P. H. 2001, MNRAS, 326, 695
Luhman, K. L. 1999, ApJ, 525, 466
———. 2000, ApJ, 544, 1044
Luhman, K. L., Rieke, G. H., Young, E. T., Cotera, A. S., Chen, H., Rieke, M. J., Schneider, G., & Thompson, R. I. 2000, ApJ, 540, 1016
Luhman, K. L., Stauffer, J. R., Muench, A. A., Rieke, G. H., Lada, E. A., Bouvier, J., & Lada, C. J. 2003, ApJ, in press
Mac Low, M.-M., & Klessen, R. 2003, Rev. Mod. Phys., submitted
Madau, P., & Pozzetti, L. 2000, MNRAS, 312, L9
Madau, P., Pozzetti, L., & Dickinson, M. 1998, ApJ, 498, 106
Marchal, L., et al. 2003, in IAU Symp. 211, Brown Dwarfs, ed. E. Martín (San Francisco: ASP), in press
Marcy, G. W., Cochran, W. D., & Mayor, M. 2000, Protostars and Planets IV, ed. V. Mannings, A. P. Boss, & S. S. Russell (Tucson: Univ. Arizona Press), 1285
Martín, E. L, Zapatero Osorio, M. R., Barrado y Navascues, D., Béjar, V., & Rebolo, R. 2001, ApJ, 558, L117
Massey, P. 1998, in ASP Conf. Ser. 142, The Stellar Initial Mass Function, ed. G. Gilmore & D. Howell (San Francisco: ASP), 17
Méra, D., Chabrier, G., & Schaeffer, R. 1996, Europhys. Lett., 33, 327
———. 1998, A&A, 330, 937
Meylan, G. 1987, A&A, 184, 144
Miller, G., & Scalo, J. 1979, ApJS, 41, 513 (MS79)
Monet, D., Dahn, C., Vrba, F., Harris, H., Pier, J., Luginbuhl, C., & Ables, H. 1992, AJ, 103, 638
Moraux, E., Bouvier, J., Stauffer, J., & Cuillandre, J.-C. 2003, A&A, 400, 891
Motte, F., & André, P. 2001, A&A, 365, 440
Motte, F., André, P., & Neri, R. 1998, A&A, 336, 150
Myers, P. C. 1998, ApJ, 496, L109
Najita, J., Tiede, G., & Carr, J. 2000, ApJ, 541, 977
Nakamura, F., & Umemura, M. 2002, ApJ, 569, 549
Nakano, T. 1966, Prog. Theor. Phys., 36, 515
———. 1998, ApJ, 494, 587
Nakano, T., Hasegawa, T., & Norman, C. 1995, ApJ, 450, 183
Nordlund, Å., & Padoan, P. 2002, in Simulations of Magnetohydrodynamic Turbulence in Astrophysics: Recent Achievements and Perspectives, ed. E. Falgarone & T. Passot (Berlin: Springer)
Onishi, T., Mizuno, A., Kawamura, A., Tachihara, K., & Fukui, Y. 2002, ApJ, 575, 950
Oppenheimer, B. R., Hambly, N. C., Digby, A. P., Hodgkin, S. T., & Saumon, D. 2001, Science, 292, 698
Ostriker, E., Gammie, C., & Stone, J. 1999, ApJ, 513, 259
Padoan, P. 1995, MNRAS, 277, 377
Padoan, P., Boldyrev, S., Langer, W., & Nordlund, Å. 2003a, ApJ, 583, 308
Padoan, P., Jimenez, R., Nordlund, Å., & Boldyrev, S. 2003b, preprint (astro-ph/0301026)
Padoan, P., Juvela, M., Goodman, A., & Nordlund, Å. 2001a, ApJ, 553, 227
Padoan, P., & Nordlund, Å. 1999, ApJ, 526, 279
———. 2002, ApJ, 576, 870
Padoan, P., Nordlund, Å., & Jones, B. 1997, MNRAS, 288, 145
Padoan, P., Nordlund, Å., Rögnvaldsson, Ö. E., & Goodman, A. 2001b, in ASP Conf. Ser. 243, From Darkness to Light: Origin and Evolution of Young Stellar Clusters, ed. T. Montmerle & P. André (San Francisco: ASP), 279
Paresce, F., & De Marchi, G. 2000, ApJ, 534, 870
Popov, S. B., Colpi, M., Prokhorov, M. E., Treves, A., & Turola, R. 2000, ApJ, 544, L53
Popper, D. M. 1980, ARA&A, 18, 115
Portinari, L., Sommer-Larsen, J., & Tantalo, R. 2003, MNRAS, in press
Pulone, L., De Marchi, G., Paresce, F., & Allard, F. 1998, ApJ, 492, L41
Reid, I. N. 1999, ARA&A, 37, 191
Reid, I. N., & Gizis, J. E. 1997, AJ, 113, 2246
Reid, I. N., Gizis, J. E., & Hawley, S. L. 2002, AJ, 124, 2721
Reid, I. N., et al. 1999, ApJ, 521, 613
Reipurth, B., & Clarke, C. 2001, AJ, 122, 432
Sahu, K. C. 1994, Nature, 370, 275

Salim, S., Lépine, S., Rich, R. M., & Shara, M. M. 2003, ApJ, 586, L149
Salpeter, E. E. 1955, ApJ, 121, 161
Saumon, D., Hubbard, W. B., Burrows, A., Guillot, T., Lunine, J. I., & Chabrier, G. 1996, ApJ, 460, 993
Scalo, J. M. 1986, Fundam. Cosmic Phys., 11, 1
Schmidt, M. 1959, ApJ, 129, 243
Ségransan, D., Kervella, P. Forveille, T., & Queloz, D. 2003a, A&A, 397, L5
Ségransan, D., et al. 2003b, in IAU Symp. 211, Brown Dwarfs, ed. E. Martín (San Francisco: ASP), in press
Shu, F. H., Adams, F. C., & Lizano, S. 1987, ARA&A, 25, 23
Siess, L., Livio, M., & Lattanzio, J. 2002, ApJ, 570, 329
Silk, J. 1977, ApJ, 214, 152
———. 1995, ApJ, 438, L41
Sommer-Larsen, J., & Dolgov, A. 2001, ApJ, 551, 608
Sommer-Larsen, J., & Zhen, C. 1990, MNRAS, 242, 10
Soubiran, C., Bienaymé, O., & Siebert, A. 2003, A&A, 398, 141
Testi, L., & Sargent, A. I. 1998, ApJ, 508, L91
Tinney, C. G., Mould, J. R., & Reid, I. N. 1993, AJ, 105, 1045
Udry, S., Mayor, M., & Queloz, D. 2003, in ASP Conf. Ser. 294, Scientific Frontiers in Research on Extrasolar Planets, ed. D. Deming & S. Seager (San Francisco: ASP), in press
White, R. J, & Basri, G. 2003, ApJ, 582, 1109
White, R. J., Ghez, A. M., Reid, I. N., & Schultz, G. 1999, ApJ, 520, 811
Worthey, G., Faber, S. M., & Gonzalez, J. J. 1992, ApJ, 398, 69
Wyse, R. 1997, ApJ, 490, L69
Wyse, R., Gilmore, G., Houdashelt, M., Feltzing, S., Hebb, L., Gallagher, J., & Smecker-Hane, T. 2002, NewA, 7, 395
Zapatero Osorio, M. R., Béjar, V. J. S., Martín, E. L., Rebolo, R., Barrado y Navascues, D., Bailer-Jones, C., & Mundt, R. 2000, Science, 290, 103
Zheng, Z., Flynn, C., Gould, A., Bahcall, J. N., & Salim, S. 2001, ApJ, 555, 393
Zinnecker, H. 1984, MNRAS, 210, 43
Zoccali, M., Cassisi, S., Frogel, J., Gould, A., Ortolani, S., Renzini, A., Rich, M., & Stephens, A. 2000, ApJ, 530, 418
Zucker, S., & Mazeh, T. 2001, ApJ, 562, 1038